Spring 2000

The Static Thrust Characterization of the Quatra Aerrow Q100XL Engine for Flight Performance Prediction of the 1/3-scaled Cessna 172P Model

Joon Fui Ho
Embry-Riddle Aeronautical University - Daytona Beach

THE STATIC THRUST CHARACTERIZATION OF THE QUATRA AERROW Q100XL ENGINE FOR FLIGHT PERFORMANCE PREDICTION OF THE 1/3-SCALE CESSNA 172P MODEL

by

Joon Fui, Ho
Master of Science in Aerospace Engineering

A Thesis Submitted to the Aerospace Engineering Department in Partial Fulfillment of the Requirements for the Degree of Master of Science in Aerospace Engineering

Embry-Riddle Aeronautical University
Daytona Beach, Florida
Spring 2000

THE STATIC THRUST CHARACTERIZATION OF THE QUATRA AERROW Q100XL ENGINE FOR FLIGHT PERFORMANCE PREDICTION OF THE 1/3-SCALE CESSNA 172P MODEL

by

Joon Fui, Ho
Master of Science in Aerospace Engineering

This thesis was prepared under the direction of the candidate's thesis committee chair, Dr. James G. Ladesic, Department of Aerospace Engineering, and has been approved by the members of his thesis committee. It was submitted to the Department of Aerospace Engineering and was accepted in partial fulfillment of the requirements for the degree of Master of Aerospace Engineering.

THESIS COMMITTEE

Dr. James G. Ladesic

Professor Charles N. Eastlake

Dr. R. Luther Reisbig

MAE Graduate Program Chair

Department Chair, Aerospace Engineering

ACKNOWLEDGEMENTS

First of all, I would like to express my gratitude to be given the opportunity to get involved in this fascinating research project. This project has made me a much better engineer and provided insights that should help make me a better analyst engineer in all aspects. One important thing I learned and valued the most is to be persistent and patient in finding the facts in a research project.

I also wishes to express my special thanks to the thesis committee chair Dr. Ladesic, and Professor Eastlake for their countless hours giving helpful counsel and practical suggestions which were the major contributions and foundation to the success of this research. Also, two wonderful people I would like to express my sincere thanks to were Aerospace Engineering Technicians, Donald Bouvier and Mike Potash. Their help in setting up all the required test equipments and insuring their proper functionality were crucial to obtain all the necessary data required for this research.

This statement of acknowledgement would be incomplete without a formal expression of sincere appreciation and gratitude to both the author's friends and family for providing the assistance and encouragement needed to complete this research project.

ABSTRACT

Author: Ho, Joon Fui

Title: The Static Thrust Characterization of the Quatra Aerrow Q100XL Engine for Flight Performance Prediction of the 1/3-scaled Cessna 172P Model

Institution: Embry-Riddle Aeronautical University

Degree: Master of Science in Aerospace Engineering

Year: 2000

The purpose of this research is to predict the thrust as a function of forward flight velocity required for the one-third-scaled Cessna 172P. This model was designed to verify scaling laws. Therefore, it is important that it be aerodynamically scaled and that it have similar thrust characteristic as that of the full scale Cessna 172P. Several propellers and two Quatra Aerrow Q100XL two-cycle engines were acquired for this research project. Three propellers were selected to undergo a series of static thrust testing. The measured static thrust was then used to predict the flight performance of each tested propellers with the use of the computer programs (ROTOR and ROTOR II). A prediction of the anticipated flight performance of the propulsion system was obtained. Using the data of this research a suitable propeller will then be selected for the flight test model, based on the flight envelope and flight condition of the flight tests.

Table of Contents

List of Tables

List of Figures

1.0 Introduction

This research project is part of a one-third-scaled fully instrumented flight test model that is designed to verify and validate scaling laws. Former graduate student Michael Hinton completed the major structure of the model, and Matti Hirvonen completed the data acquisition system that was installed on board the model. Fiberglass skin panels, fuselage fairings, wing struts, air-data-boom, and flight control systems were installed between May and December of 1999. The model is near completion at this stage (see **Figure 1** and **2**), additional pictures of the model at different construction stages were attached in **Appendix G**.

However, before flight testing the model, a detailed engine performance analysis with different types of propellers is necessary to ensure the success of the first test flight, as well as to minimize the chance of losing the model in flight due to the failure of the propulsion system.

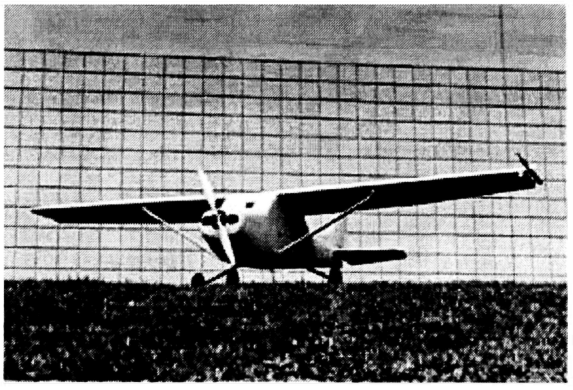

Figure 1 1/3-scaled model of Cessna 172P

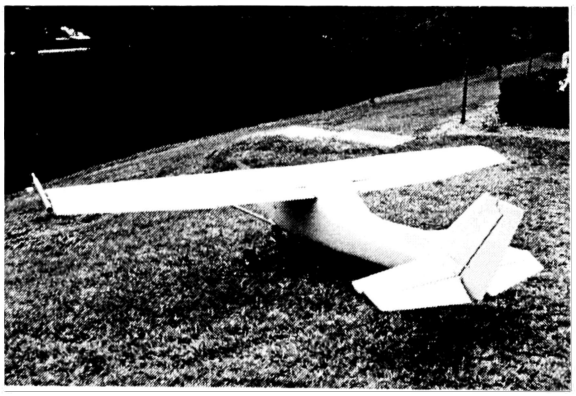

Figure 2 Look down view of the 1/3-scaled model of Cessna 172P

A series of static thrust engine tests has been conducted. The objective of these tests is to characterize the static thrust attributes of different propeller configurations on a two-cycle engine made by Quatra Aerrow, model Q100XL. The attributes will then be adjusted using theoretical methods to predict the flight performance of different propeller-engine combinations. This engine has been selected as the propulsion system of the one-third scale Cessna 172P. Since the model is designed to verify the scaling laws, it is important that it be aerodynamically scaled and that it has similar thrust as a function of forward flight velocity as that of the full scale Cessna 172P.

The characterization of the static thrust profiles for each propeller required determination of a relationship between thrust and the engine rotational speed. A test apparatus was developed in order to obtain static thrust from such an engine. The apparatus was designed to minimize severe engine induced vibrations on associated measurement equipment yet be able to measure propeller thrust. Several parameters were monitored and recorded during the engine static thrust data collection process. These were propeller type and pitch angle, engine RPM, cylinder head temperature, fuel type (octane rating), fuel consumption, and thrust. The data obtained were used to generate thrust profiles of the propulsion system for the different configurations which were needed before model initial test flight.

It is very difficult to measure the flight performance of any propulsion system in flight. Therefore, mathematical models will be developed to adapt the static thrust profile of each tested propeller to account for different forward flight velocities. Graphs of flight performance will be generated for each tested propeller. In so doing, a propeller that matches the flight performance required of the model will result. From the predicted thrust profiles the best pitch setting of the propeller will be selected for the model based on the flight envelope and flight condition of the flight tests.

2.0 The setup of the test apparatus

The Quatra Aerrow Q100XL was acquired about two years ago. The first test run of the engine was made with it installed on the aircraft. It was clear that the vibration environment was far more extreme and severe than originally anticipated. In addition, it was not an easy task to run the engine installed on the aircraft without the help of many assistants. For instance, one person was required to secure the aircraft while running the engine, another monitored and tuned the engine, and one more person was needed to collect and measure engine parameters such as cylinder head temperature, engine rotational speed and room temperature. In light of all these factors, it was decided to break in the engine while mounted on a rigid structure that would be designed and instrumented to permit the investigation of the static thrust while also providing insights to methods of isolating the vibrations of the engine. A static thrust engine stand was specifically designed and fabricated for this purpose. Static performance of the engine for different propeller configurations would be evaluated while a separate investigation to attenuate vibrations was considered.

The test stand was designed to have the capability of measuring static thrust, cylinder head temperature, and engine rotational speed (RPM), and rate of fuel consumption. To simplify and shorten the completion of the static engine test stand, the test stand was constructed using existing equipment thus requiring the minimal amount of modification. The following table is the list of equipment and materials used for the static engine test stand and **Figure 3** illustrates its principal components.

Table 1 Parts list of the static thrust engine test stand

Parts	Description	Quantity
Static engine test stand	Part of an existing SAE static thrust engine test stand	1
Engine stand	An engine stand for a Rotax engine that used to investigate ducted fan engine configuration	1
Digital temperature scale	Omega, model HH200A	1
Thermocouple	Westberg MFG, Inc. 712-4WK 4' Type J, 0 – 700F, Thermocouple 396	1
Thermometer	Typical mercury type thermometer	1
Load cell	Hardy Scales Company, model 100-0-CT-8L-FF-2.0-100#	1
Digital load scale	Embry-Riddle Aeronautical University laboratory equipment	1
Radio	Futaba, model FP-T8UAP PCM 1024	1
Battery charger	Shumacher model MC-1, 1 amp motorcycle battery charger	1
Fuel tank	Dubro 1500cc fuel tank for gasoline engine	1
Tachometer	Tower Hobbies digital mini tach	1

Table 2 Materials list of the static thrust engine test stand

Materials	Description	Quantity
Rubber mat	2.00" x 2.00"	6
Insulation mat	3.75" x 4.00"	1
Aluminum angle	3.00" x 5.00" x 0.375", 3.75" long	2
Aluminum angle	1.50" x 1.5" x 0.375", 24.00" long	2
Aluminum plate	0.125" thick, 2.75" x 3.75"	2
Aluminum plate	0.25" thick, 7.875" x 24.00"	1
#10 bolt	Flat head	14
#10 nut		14
#10 bolt		7
#10 lock nut		7

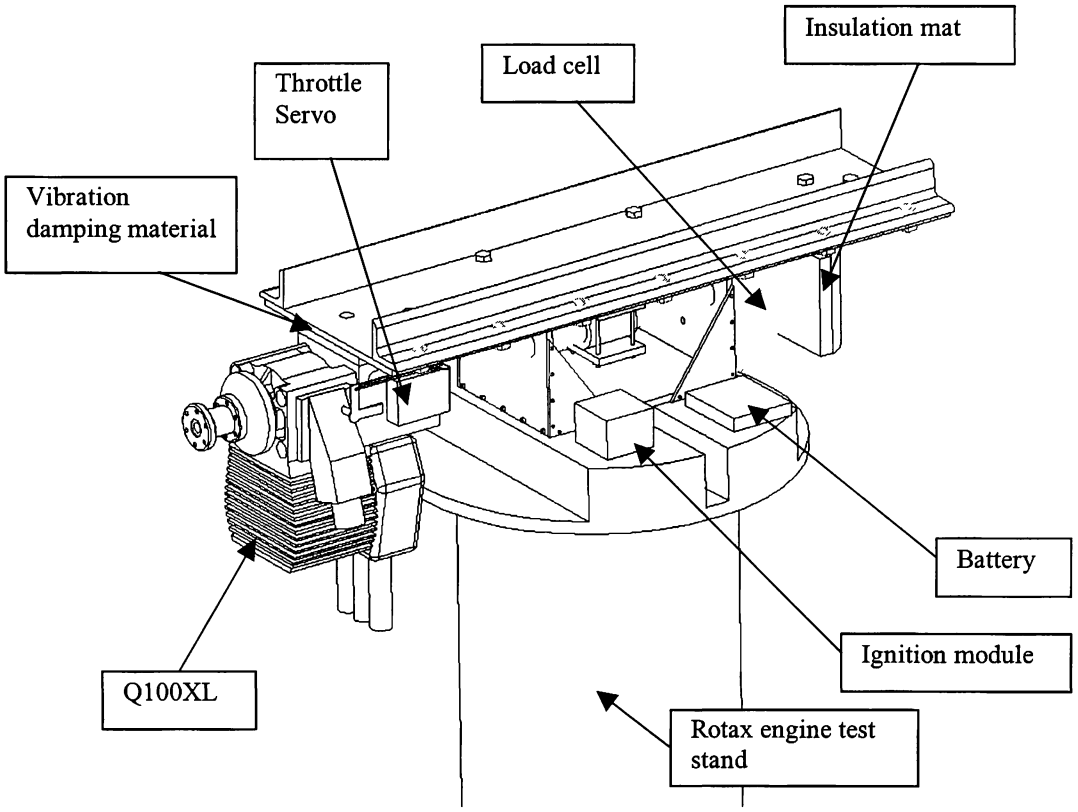

Figure 3 General setup of the static thrust engine test cell

Detail drawings and pictures of the static thrust engine test stand were attached in Appendix F.

3.0 Data Collection

Three propellers were tested during a one-and-a-half month test period. They are a Bolly G26 x 12, a Bolly G28 x 10, and a 26-inch diameter Syntec Vari-pitch prop with a round tip blade set. The original test plan was to test four different propeller acquired for this project, 2 graphite propellers made by Bolly, and 2 different blade set for the Syntec Vari-pitch prop (**Figure 4**). Three out of the four selected propellers were tested completely and successfully. During the test, one blade set of the ground adjustable pitch propeller failed during the test. This propeller is made out of hard wood, and the blade hub attachment proved to be too low in structural strength for the operational conditions. The wooden hub failed in shear, parallel to the grain, under centrifugal loading and flung a blade. No other damage to the system was sustained and there were no injuries (**Figure 5, Figure 6**). With such a serious incident on record, it was decided not to test the second set of wooden blades.

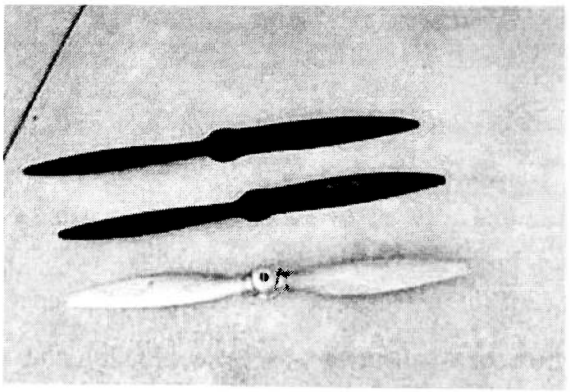

Figure 4 Tested propellers: Bolly G28x10, Bolly G26x12, Syntec Vari-Pitch (Classic Blade)

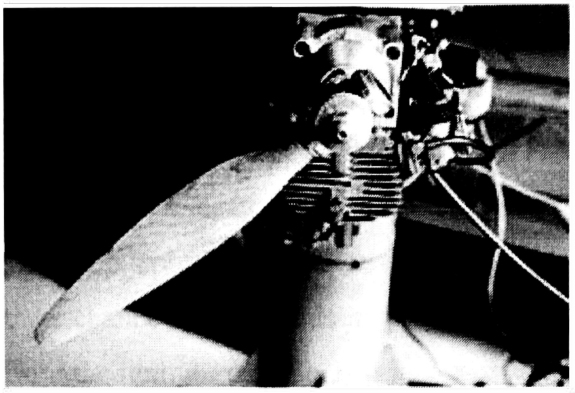

Figure 5 Structure failure of the Syntec Vari-Pitch Prop on the static engine test stand

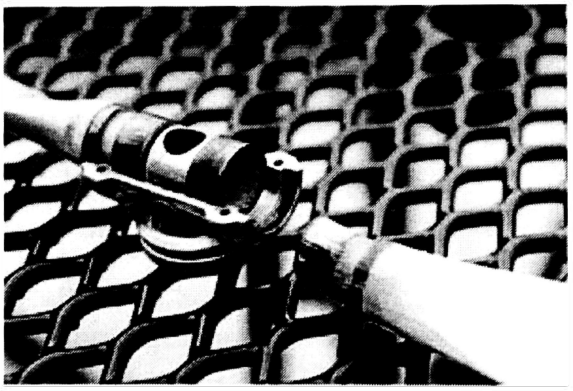

Figure 6 Details of the Syntec Vari-Pitch Prop hub assembly

Throughout the data collection process, several unexpected problems of the test apparatus and potential operator safety concerns were encountered. First, even with the careful implementation of vibration damping material, the vibration induced by the engine was still great enough to cause some problems during the test period. For instance, on different occasions the vibration had caused a failure of a load cell, induced serious fatigue cracks on the muffler assembly, and damaged the thermocouple that was used to measure the cylinder head temperature. After the incident where the muffler assembly failed, every bolt on the engine and the test stand was regularly inspected for tightness before and after each run.

Experience gained from the first engine run while installed on the aircraft indicated that the engine vibration may have caused an irregular response to the throttle. This was later determined to be due to the fact that the servo and the engine were mounted separately on the aircraft and had different planes of relative displacement. To correct the problem, the servo was relocated directly on the engine in order to avoid a long servo arm. There was also a potential of RF interference from the ignition module to the servo. To reduce the chance of RF interference an RF shielded servo wire, carefully routed away from the ignition module, was installed.

Another problem encountered during early testing was a poor mechanical connection between the ground adjustable variable pitch propeller hub and the engine. During the first run of the Syntec Vari-pitch prop, the propeller hub slipped during operation. The slippage of the propeller had caused serious metal galling between the propeller and engine hub. The failure of the connection between the propeller and the engine was primarily due to the lack of positive grip between the two components and improperly torqued bolts. In general, a typical RC engine relies on friction between the propeller and engine hub to prevent slippage. For this installation there appeared to be too close a match in material type and finish between the engine hub and the prop hub. To repair the engine hub, similar material was welded to the hub and then faced off. A small modification was done to the propeller hub assembly and the engine hub to prevent any slippage in the future. Two locking pins were installed to the hub assembly to ensure positive gripping between the propeller and the engine hub.

One of the major challenges faced during the early tests was starting the engine. The Quatra Aerrow model Q100XL engine has no self-start mechanism. Therefore, the engine required manual starting by turning the propeller either by hand or a padded stick. Throughout the whole test period, both methods had been tried and used to start the engine. Several prop strikes caused by engine backfire while starting the engine quickly cause an abandoning of hand starting. Therefore, a padded stick is found to be the most reliable and safe way to start the engine. The cause of engine backfire was eventually

diagnosed as inadequate carburetor and throttle settings. By setting the carburetor correctly, the potential of having prop strike was greatly reduced.

An issue that needed to be addressed continually was the operational safety precautions in running a 10 Hp two cycle engine. Simple static engine thrust measuring tests may not seem to pose much danger, but it is crucial that the operator keep in mind that a 10 Hp engine turning a 26-inch diameter propeller at 7000 rpm can cause serious injury to any person who is underestimates its potential.

4.0 Data analysis

Throughout the whole data collecting process, each tested propeller had two sets of readings taken under different atmospheric conditions. Due to changing atmospheric conditions throughout the test periods, all the data collected were corrected to the standard sea level conditions using information supplied by the NOAA (National Oceanic and Atmospheric Administration). Corrections included temperature, density and pressure. Sample calculations were presented in Appendix A. Final corrected thrust data were plotted against engine RPM. All the plots were presented in **Appendix A**. Additional theoretical data were produced using a computer code developed by Professor Charles Eastlake at Embry-Riddle Aeronautical University for predicting thrust as a function of propeller rotational speed.

Of all the data collected, the data for the graphite propellers made by Bolly displayed some curious attributes. There were two sets of data for each of the tested graphite propellers and some differences in the setup of the test apparatus for each. The graph of corrected static thrust against engine RPM for Bolly 26 x 10 propeller is shown on **Figure 7**. From the graph, the data collected on the Feb 1st 2000 was seem to have a higher measured static thrust than the data collected on the Feb 22nd 2000. Both sets of data were corrected to standard sea level condition. The major differences in the equipment setup between the two sets of data were thought to be limited to the vibration damping material used on the test equipment, and carburetor setting. However, later investigations introduced the notions that a leaking muffler also contributed to the differences observed.

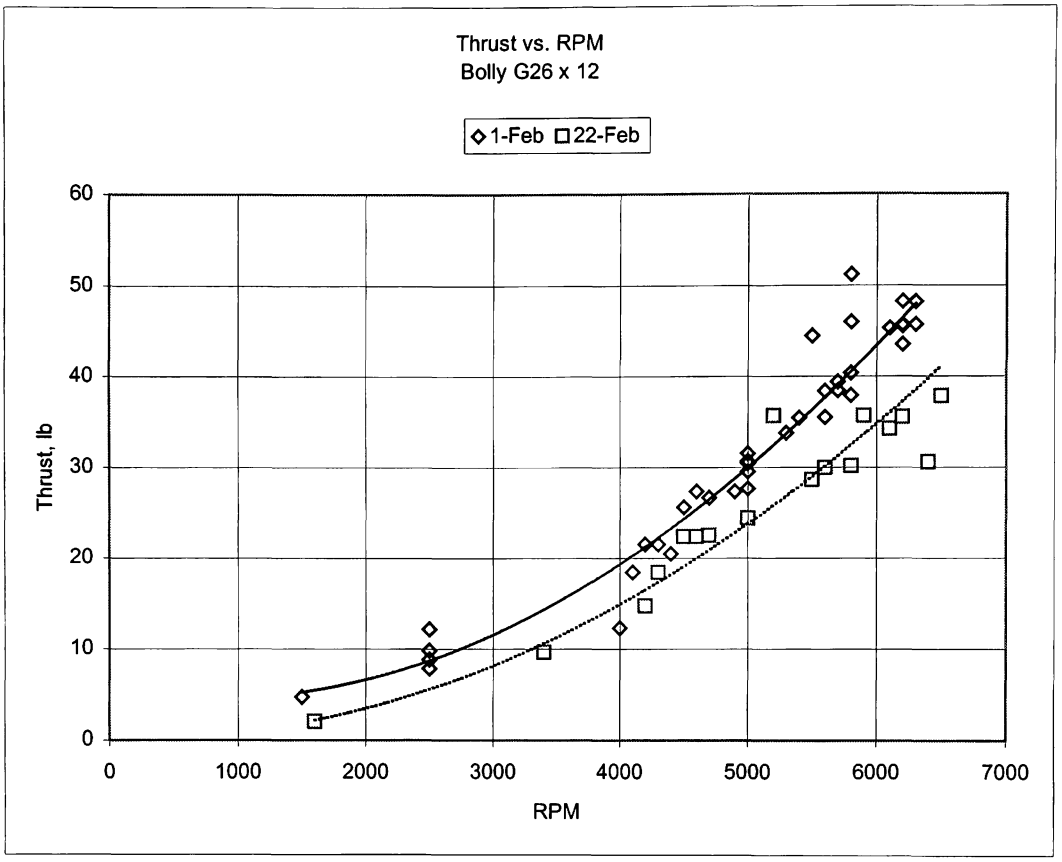

Figure 7 Thrust versus RPM curve of Bolly 26 x 12

From the plot of the data in **Figure 7**, it appears that the difference between two curves is linear. The original sources thought to be possible causes were the following:

- Improper or faulty meter readings
- Incorrect calibrated load cell installed on the engine test stand.
- Vibration induced on the measuring device of the test apparatus.
- Atmospheric conditions that are not accounted for in the process of correcting the data to standard sea level conditions.

In order to better understand the causes, additional tests were conducted to investigate the data variations. Also the calibration of the load cell was verified prior to these tests. The calibration test proved that the load cell was in proper calibration. As a result, the possibility of a bad reading from the load cell was eliminated.

The propeller that was selected for verification tests was the Bolly 26 x 12. This propeller was tested using the most recent test apparatus configurations. In other words, the test apparatus configuration was the same as that used for the data collected on the Feb 22nd 2000. Then, the propeller was tested with the apparatus setup configured as for the Feb 1st 2000 tests. Oddly, the static thrust measured on the retest was found to be comparable with the first set of data collected on Feb 1st (see **Figure 8**).

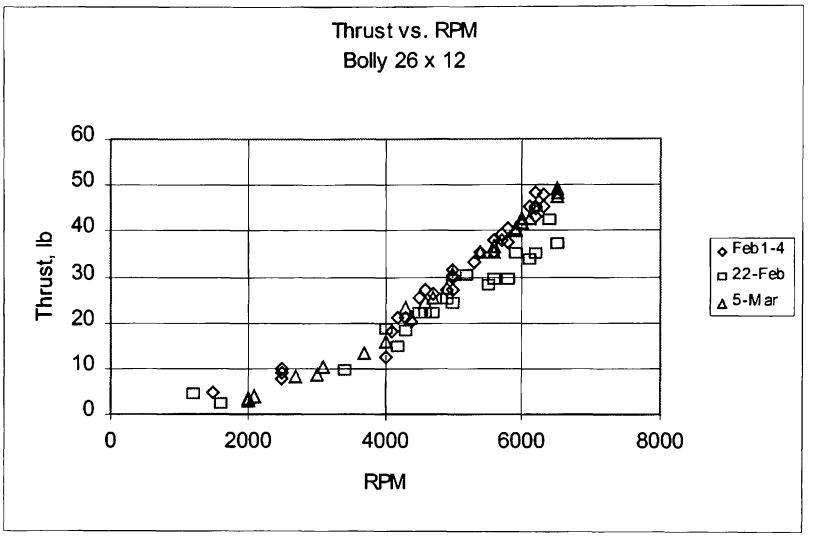

Figure 8 Plotted static thrust data of Bolly G26 x 12 on Feb 1-4, Feb 22 and Mar 5, 2000

This clearly suggests that the load cell that eventually failed was correct in calibration at the time of the earlier tests. Further, the vibration induced by the engine did have some influence on the thrust readings but not enough to account for the large differences. From the thrust versus engine RPM curves of **Figure 9**, two sets of data were plotted. One data set was obtained with high vibration damping setup. Conversely, the second data set was obtained with low vibration damping setup. The difference in vibration damping setup had caused a difference in two pounds measured static thrust. The defect that may have been caused by the engine-induced vibrations on the measuring device may had been greater during the earlier testes because the engine was subsequently tuned. As a result, it was not possible to recreate exactly the same environment as that of the measuring device from earlier runs. While repeating tests to investigate the differences of the test data for Bolly 26 x 10, a different octane rating gasoline was also tested to investigate the beneficial of running the engine with higher

octane rated gasoline. The entire test data collected previously took place with the engine running on 87-octane rating gasoline. Two of the tests used 93-octane gasoline. There appears to be an inverse relationship between thrust produced at RPM and the octane rating (see **Figure 10**). Although the performance of the engine degraded slightly while running the 93-octane rating gasoline, perceptively the engine had a better throttle response and throttle transition. This is one aspect that will require further exploration.

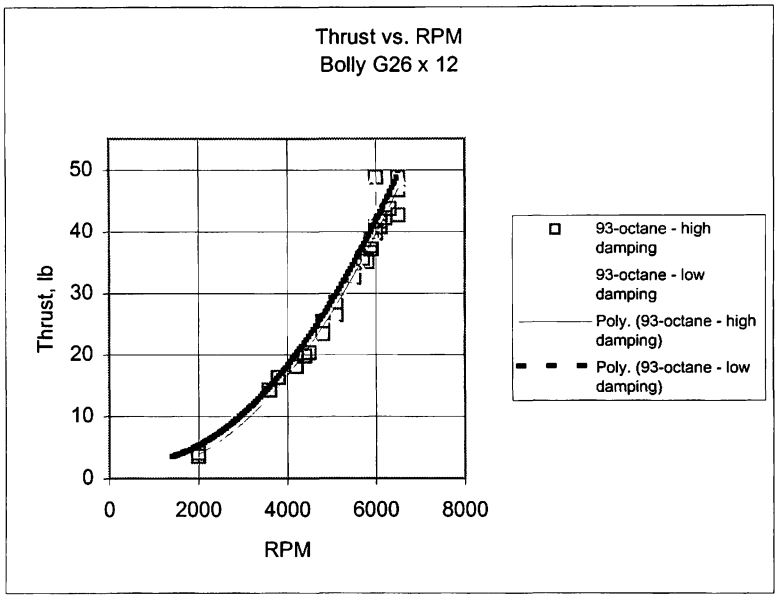

Figure 9 Static thrust comparison between hard and soft rubber setup on the engine mount

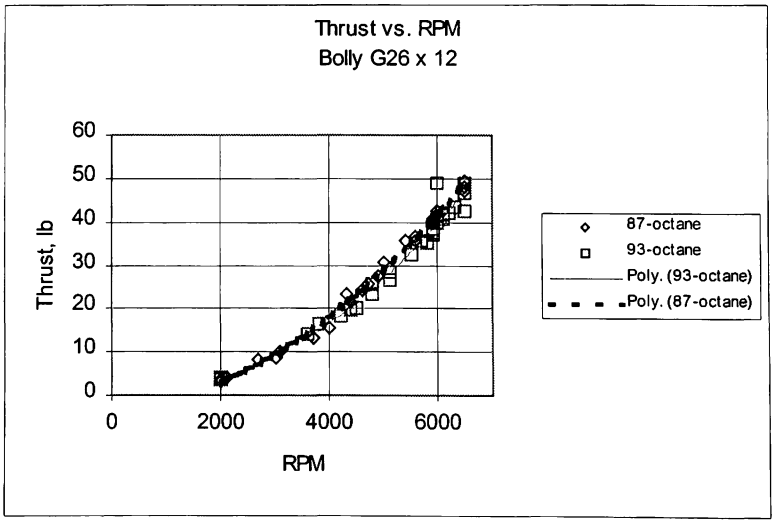

Figure 10 Static thrust comparisons between 87 and 93 octane

There is one factor that may not be resolved by simply conducting additional tests. This is the variation of atmospheric conditions and the effect they may have on the engine performance. It was not anticipated that atmospheric conditions variations would have a great influence to the engine performance. Thus, atmospheric conditions such as the barometric pressure and relative humidity were not measured during the test. To investigate the sensitivity barometric pressure had on the thrust produced, a set of data was chosen and corrected by varying barometric pressure 4% to 30 in-Hg. It was found that the change of barometric pressure did have a small effect on end data (see **Figure 10**).

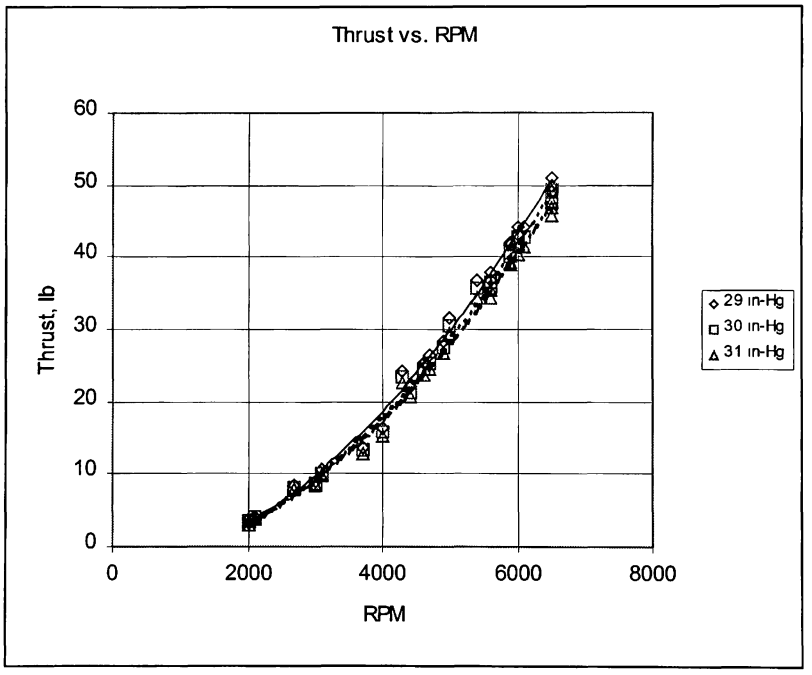

Figure 11 Thrust versus RPM curve with different barometric pressure

In order to have all the data corrected to the standard sea level conditions, a real atmospheric condition reading is required to fully investigate the effect of such variations. A set of weather data for Daytona Beach atmospheric conditions from January 1st to March 9 of 2000 was obtained from the NOAA (National Oceanic and Atmospheric Administration). From the weather data of Daytona Beach atmospheric conditions, the variation of the barometric pressure was found to be around 0.4 in-Hg throughout the test period. Barometric pressures for each tested day that were obtained

from the NOAA were used to correct the measured data. The correction cause by the variation of 0.4 in-Hg was about 0.6 lb, which is far less than the deviation of the data collected during the experiments. The correction of barometric pressure and temperature on the experimental data had included the effect of the change of relative humidity. Therefore the correction of relative humidity on the experimental data was not needed. After all these possible causes of the difference in measured data were investigated, another possibility came to light that there may have an even larger effects on engine performance than any of the others.

Tracing back through the engine log, there were a few incidents where the muffler assembly vibrated loose and fell apart during a test. Before commencing with the re-tests, some repair of the muffler assembly was needed. There were cracks and deformations on the body of the muffler assembly. The muffler was carefully reshaped and sealed with gasket sealer before being reinstalled on the engine. To further identify the magnitude of the contribution to the discrepancies of a leaking muffler would make, a test was conducted where the muffler was purposely allowed to leak and thrust measurement were made. From the tests, with a leaking exhaust system, the measured thrust was 2 - 3 lb lower than a non-leaking exhaust system. A leaking exhaust system was also responsible for engine roughness. All these investigations concluded that a leaking muffler had the greatest impact to the engine performance. **Table 3** lists all the possible instrumentation and human uncertainty that might have affected the measured experimental data. In addition, from **Table 3** the reading uncertainty of a typical thermometer was found to have an uncertainty of ±5°F. The five degree Fahrenheit difference led to thrust correction of 0.2 lb, which was considerably smaller than the other uncertainties imposed on the data.

Table 3 Sources of uncertainty

Sources of uncertainty	Uncertainty
Thermometer	: ±5°F ⇒ ±0.2 lb
Barometric pressure	: ±0.6 lb
Load scale (engine vibration)	: ±2.0 lb
Leaking exhaust	: ±3.0 lb
RPM	: ±200RPM
Total uncertainty	**: ±5.8 lb**

The uncertainties founded were then imposed on the experimental data of Bolly 26 x 12 propeller (see **Figure 11**). With a total uncertainty of 5.8 lb introduce to the data collected on February 22nd, the data points were brought closer to the other two sets of data obtained on Feb 1st and Feb 22nd. Additional plots were presented in **Appendix A.**

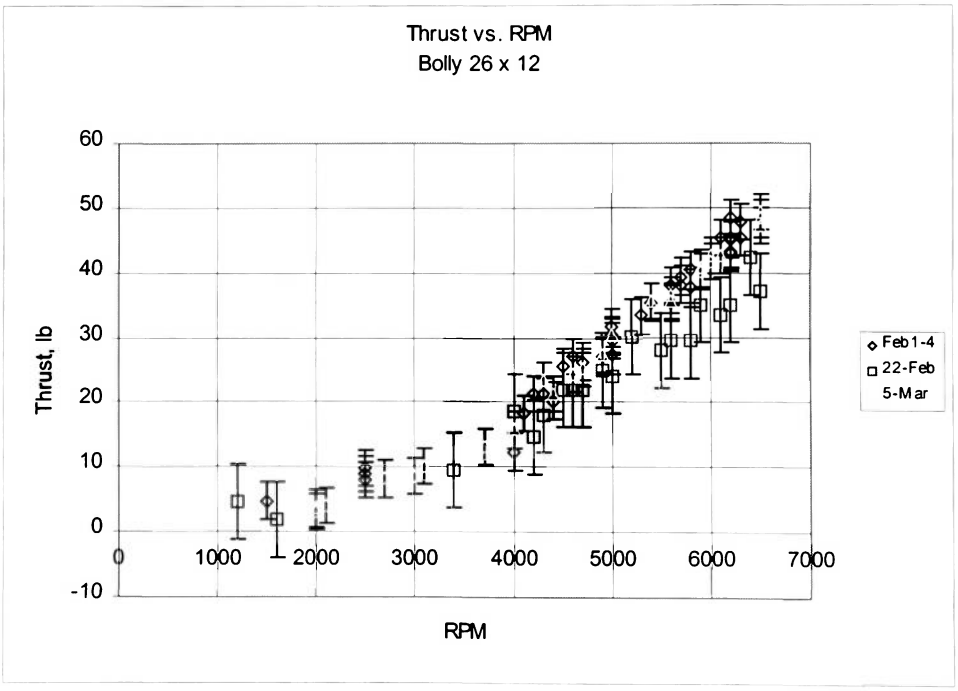

Figure 12 Graph of thrust versus RPM curve of Bolly G26x12 with uncertainty

5.0 Flight performance prediction

The computer program, entitled "ROTOR" developed by Professor Charles N. Eastlake was selected to predict the theoretical flight performance of the tested propeller. This program utilizes momentum and blade-element theory to calculate the angle of attack distribution along the span of a rotating airfoil, and then calculates the thrust produced and the power required to rotate it. The ROTOR program is designed to use as a tool for the design of both propellers and helicopter rotors. In order to run the program, geometrical information of the propeller is required. The details of the input parameters are listed in **Table 4**.

Table 4 Input parameters of ROTOR program

	Input parameters	Units
1	Forward velocity	ft/s
2	Propeller diameter	inch
3	Propeller RPM	RPM
5	Number of blade	
6	Radial position, r/R	in/in
7	Local chord length	In
8	Chord geometrical pitch angle	degree
9	2-D lift curve slope of blade airfoil	1/radian
10	Airfoil zero lift angle of attack	degree
11	Repeat step 6 through 10 four times	

To use the ROTOR program in this research, geometrical information was obtained directly from the propellers tested. Geometrical information was taken from five different spanwise locations along the blade for each tested propeller. The measured geometrical information of the propellers that were used as input for the ROTOR program are listed in the following table.

Table 5 Geometrical information of Bolly G28x10, Bolly G26x12 and Syntec Vari-Pitch Prop (Classic blade design)

Bolly G28 x 10

R, in	Chord, in	r/R	β (degree)
3	1.875	0.214286	25.7562
5.5	2	0.392857	17.9576
8	1.9375	0.571429	12.41449
11	1.5	0.785714	8.162256
14	0.375	1	5.855401

Bolly G26 x 12

R, in	Chord, in	r/R	β (degree)
2.5	1.75	0.192308	27.20289
5	1.9375	0.384615	19.60196
7.5	1.875	0.576923	15.46601
10	1.5	0.769231	11.53696
13	0.375	1	9.206896

Syntec Vari-pitch 26" (classic blade)

R, in	Chord, in	r/R	β (degree)
4	1.875	0.307692	13.88654
6.5	2	0.5	7.180756
9	1.75	0.692308	4.588566
11	1.375	0.846154	3.126776
13	0.5	1	2.292443

Without knowing the exact airfoil shapes used by the propeller manufacturer, a good educated guess as to correct zero lift angle of attack was necessary. Based on some research on airfoils generally used on propellers, the zero lift angle of attack was taken in the range of -2° to -4°. The measured geometry was used as input to the program several times with different zero lift angles of attack until a zero lift angle in the selected range was found match to the experimental data. The zero lift angle found for each propellers were –4° for Bolly G28 x 10, -3.5° for Bolly G26 x 12 and -3° for Syntec Vari-Pitch Prop. The predicted thrust output of the program was found to have good agreement with that of the experimental measured thrust for each respective propeller. The following graphs are the thrust versus RPM curve of the Syntec Vari-pitch prop at pitch setting 8 and 9. **Figure 13** and **Figure 14** clearly show that the curve predicted by ROTOR is in close agreement with the experimental data.

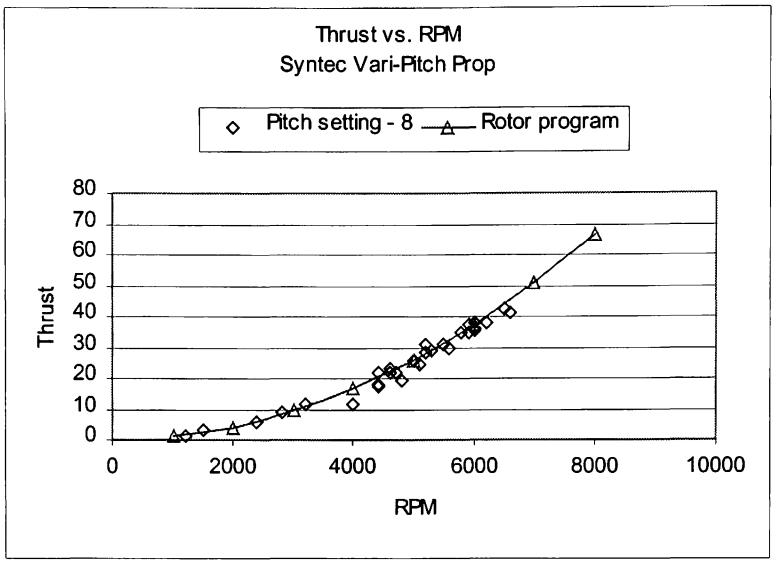

Figure 13 Comparing the thrust prediction of ROTOR program with experimental data of Syntac Vari-Pitch prop

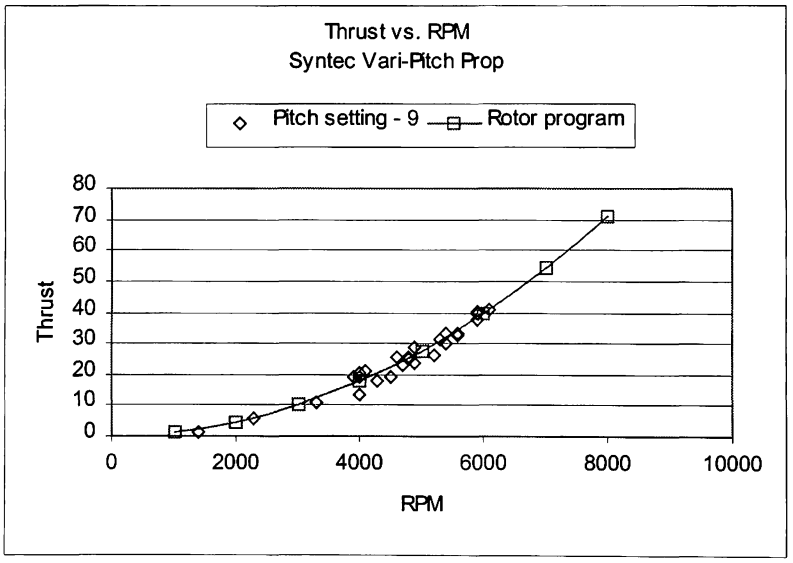

Figure 14 Comparing the thrust prediction of ROTOR program with the experimental data of the Syntec Vari-Pitch prop

On the other hand, the power required to drive the propeller is slightly under predicted (see **Figure 16**). A discussion with Professor Eastlake led to speculation that the possible cause may have been due to the drag equation used in the computer program which may not be suitable for the current application. The reason is that the drag equation used in the ROTOR program is based on a Reynold's number of three million or above. In contrast, the tested propellers operated at much lower Reynold's number

around 500,000. In order to obtain better power prediction from the program, a small change to the drag equation was proposed as follows:

$$\mathrm{Re}(x) = \frac{(r\Omega_x)C_x}{\upsilon}$$

$$DragCF = \left[\frac{3000000}{\mathrm{Re}(x)}\right]^{0.2} \qquad \textit{Equation 5.1}$$

Ω	: Rotational speed
C_x	: Chord length at r
r	: Radial location of C_x
ν	: Kinematic viscosity
DragCF	: Drag correction factor

In order to define a drag correction factor, the Reynold's number was calculated for each blade section at a different RPM. The Reynold's number was than used to compute the drag correction factor based on the *Equation 5.1*. This equation was adopted from the AE309 Lecture Notes and Laboratory Manual prepared by Professor Eastlake. Since there will be five calculated drag correction factor for each RPM, the correction factor was averaged at each respective RPM. A graph of drag correction factor against engine rotational speed was plotted (see **Figure 15**). From the graph, trend-lines were obtained, and then implemented in the ROTOR program. A sample calculation of the drag correction factor was attached in **Appendix B**. It is worth noting that the 1.6 – 2.0 correction factor applied only to profile power. Induced power is significantly larger than profile power, as the increase in total power due to the correction factor is relatively small.

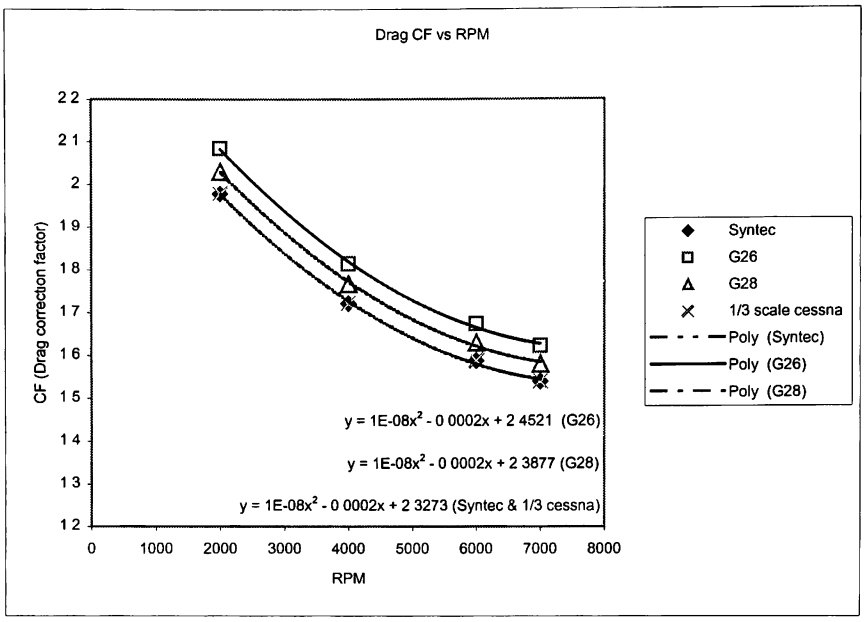

Figure 15 Drag correction factor plot against propeller rotational speed

With the drag correction factor implemented in the ROTOR program, the predicted power require was more in agreement with the power available curve provided by the engine manufacturer (see **Figure 16**).

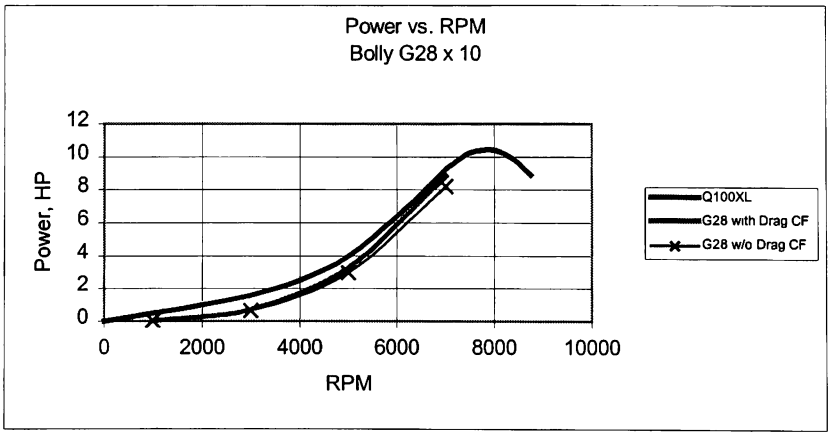

Figure 16 Graph of power required of Bolly G28x10 with & without drag correction factor introduced to the drag equation in the ROTOR program

5.1 Development of ROTOR II

A minor flaw was found in the ROTOR program. ROTOR was not giving accurate output as the forward flight velocity increases on the propeller. After careful examination of the ROTOR code, the equation that used to calculate the induced velocity was found to be inaccurate. Equation 5.2 was the equation used in the ROTOR code. This equation does not account for the forward flight velocity. Therefore, the calculated portion of the in-flow angle attributed to the induced velocity does not decrease as the forward flight velocity increases. This causes total in-flow angle to be too large, in turn resulting in the blade element angle of attack being increasingly too small as forward flight velocity increases.

$$v_i = \left[\frac{\sigma(x)a\Omega R}{16}\right]\left[\sqrt{1+\frac{2(\beta x\Omega R)}{\frac{\sigma(x)a\Omega R}{16}}}\right] \qquad \textit{Equation 5.2}$$

$$v_i = \left[\frac{V_f}{2}+\frac{\sigma(x)a\Omega R}{16}\right]\left[-1+\sqrt{1+\frac{2(\beta x\Omega R - V_f)}{\frac{4V_f{}^2}{\sigma(x)a\Omega R}+V_f+\frac{\sigma(x)a\Omega R}{16}}}\right] \qquad \textit{Equation 5.3}$$

To enhance the versatility and accuracy of the ROTOR program, it was converted from QBasic to an Excel Spreadsheet. The new program used the same equations as the original ROTOR program except for the equation that was used to calculate in-flow velocity. Instead of using *Equation 5.2*, *Equation 5.3* was implemented in the ROTOR II code. A few new features were added to the program. For instance, the new program will produce the output of advance ratio (J), allow the user to change the density altitude, and allow change in the pitch angle of the blade. With the computation capability and flexibility of the Excel spreadsheet, these analyses were accomplished in an efficient and timely manner. The following is the list of equations used in ROTOR II. Most of these equations are derived in *Aerodynamics of the Helicopter* by Gessow and Meyers[6].

$$\Omega = RPM\frac{2\pi}{60}$$

$$X = \frac{r}{R}$$

$$\sigma(x) = \frac{bC_v}{\pi R}$$

$$v_i = \left[\frac{V_f}{2} + \frac{\sigma(x)a\Omega R}{16}\right]\left[-1 + \sqrt{1 + \frac{2(\beta x\Omega R - V_f)}{\frac{4V_f^{\,2}}{\sigma(x)a\Omega R} + V_f + \frac{\sigma(x)a\Omega R}{16}}}\right]$$

$$\phi(x) = \tan^{-1}\left[\frac{v_i + V_f}{\Omega R x}\right]$$

$$AR = \frac{\frac{D}{2}}{C_{average}}$$

$$CORR = \frac{AR}{AR + 2}$$

$$\alpha = \beta - \alpha_0 - \phi$$

$$C_L = CORR\ \ a\alpha$$

$$C_{do} = 0\ 0107 - 0\ 151\alpha + 1\ 72\alpha^2$$

$$C_d = \phi\ \ C_L$$

$$dT = b\ \ \frac{1}{2}\rho(\Omega r)^2 C\ \ C_L dr$$

$$dQ = b\ \ \frac{1}{2}\rho(\Omega r)^2 C(C_{do} + C_{di})rdr$$

$$P = \Omega Q$$

$$\eta = \frac{TV}{P}$$

$$J = \frac{V}{nD}$$

Ω	*Propeller rotational speed in rad s* ^{1}
X	*Normalized blade chord section by radius of the propeller*
$\sigma(x)$	*Blade solidity*
v_i	*Inflow velocity*
$\phi(x)$	*In flow angle*
AR	*Aspect ratio of the blade*
$CORR$	*Correction factor on* C_L *based on blade aspect ratio*
α	*Angle of attack*
C_L	*Lift coefficient*
C_{d0}	*Profile drag coefficient*
C_{di}	*Induce drag coefficient*
dT	*Sectional thrust*
dQ	*Sectional Torque*
P	*Power*
η	*Propeller efficiency*
J	*Advance ratio*

To ensure there was no significant flaw in the program, the results of the ROTOR II were compared and verified with these of ROTOR at zero forward velocity. The comparisons between the two programs are displayed in the following graphs. Additional data are attached in **Appendix C**.

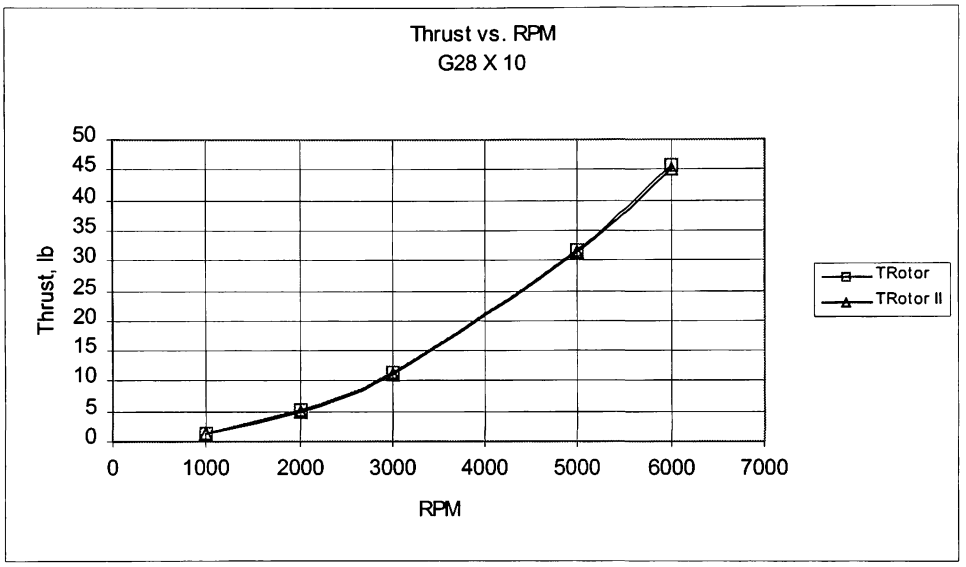

Figure 17 Static thrust prediction of ROTOR & ROTOR II of Bolly G28x10

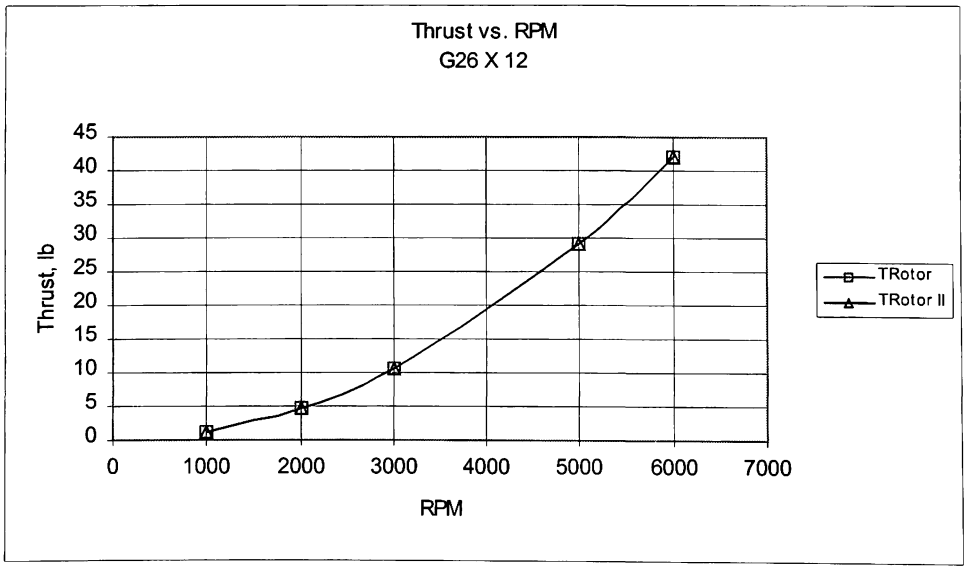

Figure 18 Static thrust prediction of ROTOR & ROTOR II of Bolly G26x12

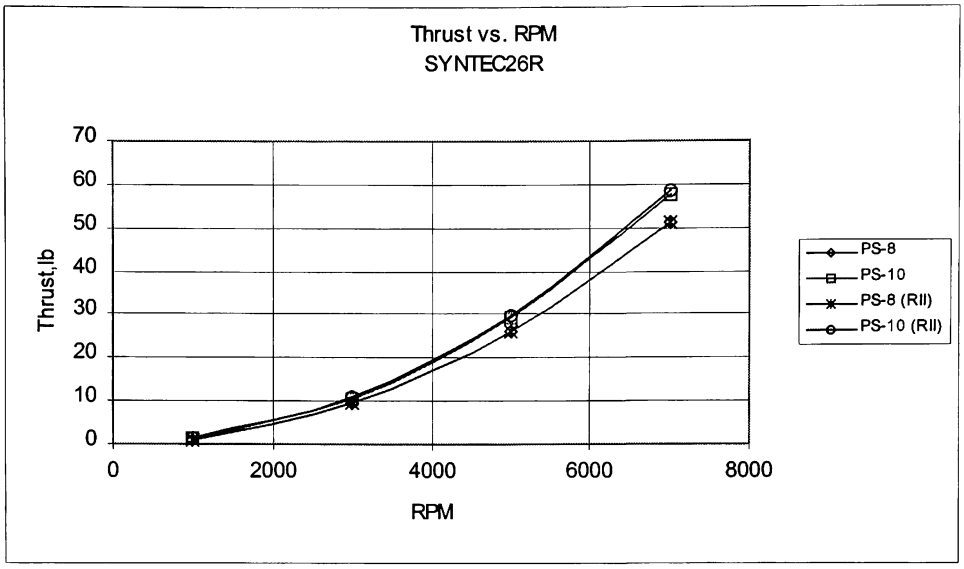

Figure 19 Static thrust prediction of ROTOR & ROTOR II of Syntec Vari-Pitch Prop at pitch setting 8 & 10

6.0 Scaling laws

As stated earlier, this research was conducted to obtain populsion information for the model prior to flight-testing. The main goal of this flight-testing will be used to compare the flight performance of a carefully geometrically scaled model with its full-scale counterpart. The proposed outcome of this research will hopefully lead to the development of a scaled model single engine pusher general aviation aircraft based on the design created by the senior design students of Aerospace Engineering from Embry-Riddle Aeronautical University. This airplane won the AGATE design competition in 1996.

To obtain accurate results from the dynamic model, it is necessary for the model to be dimensionally similar in all aspects to the full-scale counterpart. They must not only be geometrically to scale, but must also have gross weight, moment of inertia, power accelerations, all aerodynamic forces and moments to scale. If all the scaling were done properly, the model should perform every maneuver of the full-scale aircraft at rates of that reflect the actual prototype motions. A scale principal is required. Several methods are available for scaling an aircraft appropriately. For instance, the methods of comparing dynamically similar motions initiated by Newton, Stokes (or Helmholtz) and Rayleigh respectively are available. The scaling law adopted for this project is based on Froude's Law of comparison. Ernest G. Stout[16] used this method in the development of high-speed water based aircraft in the 1950s with great success. This method will be derived and illustrated as follows.

The general resistance equation for the force acting on a body in motion, partly or fully immersed in an imperfect fluid, can be expressed in the following form:

$$R = (\rho V^2 L^2) \cdot f\left[\tau, \frac{V^2}{gL}, \frac{\rho VL}{\mu}, \frac{V}{a}, \frac{l}{L}, \frac{\upsilon}{V}, \frac{V^2 L}{\gamma}, \frac{L}{b}\right] \qquad \textit{Equation 6 1}$$

ρ	Density of the fluid
V	Velocity of the body
L	Linear size of the body
τ	Trim or angle of attack
g	Gravity
V/a	Compressibility of the fluid
l/L	Surface roughness
ν/V	Texture of the fluid flow or turbulence
γ	Surface tension
L/b	Aspect ratio

$f_1(\tau)$	Variation of resistance coefficient with trim
$f_2(V^2/gL)$	Froude number
$f_3(\rho VL/\mu)$	Reynolds number
$f_4(V/a)$	Compressibility factor
$f_5(l/L)$	Surface roughness factor
$f_6(\upsilon/V)$	Stream turbulence represented by the ratio of the average lateral turbulence velocity to the measured axial velocity
$f_7(V^2L/\gamma)$	Surface tension factor
$f_8(L/b)$	Aspect ratio factor

In the following derivations, λ will be used as a symbol for scale.

L. Length
T: Time

If the linear scale is a ratio of length,

$L \propto \lambda^{-1}$
$\therefore L_{model} = \lambda^{-1} \bullet L$

For area,

$Area = L \bullet L$
$Area \propto \lambda^{-2}$
$\therefore Area_{model} = \lambda^{-2} \bullet Area$

Similarly, a volume or mass is an area, L^2, multiplied by the thickness or height L.

$Volume = Area \bullet L$
$Volume \propto \lambda^{-3}$
$\therefore Volume_{model} = \lambda^{-3} \bullet Volume$

Since volume is directly proportional to mass,

$Volume \propto Mass$
$\therefore Mass_{model} = \lambda^{-3} \bullet Mass$

Based on Froude's law of Comparison, from equation (6.1) the expression for the velocity varying with the square root of the linear dimension.

$$F = \frac{V^2}{gL}$$

$Velocity \propto \sqrt{L}$
$Velocity \propto \lambda^{-1/2}$
$Velocity_{model} = \lambda^{-1/2} \bullet Velocity$

Velocity has components of distance traveled with respect to time,

$Velocity = L / T$
$T = L / Velocity$
$T = L / \sqrt{L}$
$T \propto \lambda^{-1/2}$
$\therefore T_{model} = \lambda^{-1/2} \bullet T$

For engine rotation speed, since revolutions are non-dimensional,

$Acceleration = L / T^2$
$RPM \propto 1 / T$
$RPM \propto \lambda^{1/2}$
$\therefore RPM_{model} = \lambda^{1/2} \bullet RPM$

For angular velocity,

$\omega = V / R$ *(R: radius)*

$\omega = V / L$

$\omega \propto \sqrt{L} / L$

$\omega \propto \lambda^{1/2}$

$\therefore \omega_{model} = \lambda^{1/2} \bullet \omega$

For acceleration,

$Acceleration = L / T^2$

$Acceleration \propto L / (\sqrt{L})^2$

$Acceleration \propto 1$

$\therefore Acceleration_{model} = Acceleration$

For angular acceleration,

$\alpha = V^2 / R$

$\alpha = V^2 / L$

$\alpha \propto \sqrt{L} / L$

$\alpha \propto \lambda$

$\therefore \alpha_{model} = \lambda \bullet \alpha$

For force,

$Force = Mass \bullet Acceleration$

$Force \propto \lambda^{-3} \bullet 1$

$Force \propto \lambda^{-3}$

$\therefore Force_{model} = \lambda^{-3} \bullet Force$

For moments,

$Moment = Force \bullet Arm\ (distance)$

$Moment \propto \lambda^{-3} \bullet \lambda^{-1}$

$\therefore Moment_{model} = \lambda^{-4} \bullet Moment$

For moments of inertia,

$I = Mass \bullet Arm^2\ (distance)$

$I \propto \lambda^{-3} \bullet \lambda^{-2}$

$\therefore I_{model} = \lambda^{-5} \bullet I$

For slightly complex functions such as work and power, the same procedure can be used. Work is defined as force times the distance traveled,

$Work = Force \bullet distance\ traveled$

$Work \propto \lambda^{-3} \bullet \lambda^{-1}$

$\therefore Work_{model} = \lambda^{-4} \bullet Work$

Power is defined as the work done per unit time,

$Power = Work / T$

$Power \propto \lambda^{-4} \bullet \lambda^{-1/2}$

$\therefore Power_{model} = \lambda^{-7/2} \bullet Power$

The following table summarizes the fundamental relationships in condensed form. In addition, a typical set of values for the model was included.

Table 6 Dimensional conversion based on Froude's Law of Comparison

Unit	General Conversion	1/3 scale $\lambda = 3$
Linear dimensions	λ^{-1}	1/3
Area	λ^{-2}	1/9
Volume	λ^{-3}	1/27
Mass	λ^{-3}	1/27
Time	$\lambda^{-1/2}$	0.557
Linear velocity	$\lambda^{-1/2}$	0.557
Linear acceleration	Constant	1
RPM	$\lambda^{1/2}$	1.732
Angular velocity	$\lambda^{1/2}$	1.732
Angular acceleration	λ	3
Force	λ^{-3}	1/27
Moment	λ^{-4}	1/81
Moment of inertia	λ^{-5}	1/243
Work	λ^{-4}	1/81
Power	$\lambda^{-7/2}$	0.021
Wing loading	λ^{-1}	1/3
Power loading	$\lambda^{1/2}$	1.732

6.1 Application of scaling law in flight performance analysis

There are two important parameters that dictate how well an aircraft will perform in flight. They are thrust to weight ratio and wing loading. These two parameters will determine the acceleration, climb, cruise speed, and turn rate. In order to have the model flight envelope similar to that of the Cessna 172P, it is critical to have the thrust and power of the model scaled properly.

There was no experimental thrust data for the propulsion system available on the full size Cessna 172P. Thus, ROTOR II was used to predict the performance of the propeller that is installed on the prototype aircraft. The engine performance data was extracted from the 1986 Cessna 172P pilot information manual. Again, to use ROTOR II the geometrical information of propeller model 1C160/DTM7557 was obtained and measured from one of the decommissioned Cessna 172 parked at the AMT (Aviation Maintenance Technology department) of Embry-Riddle Aeronautical University. **Table 7** tabulates the geometrical information of 1C160/DTM7557 for the inputs to ROTOR II. The thrust prediction of this propeller is in **Table 8**.

Table 7 Inputs of 1C160/DTM7557 for ROTOR II

r/R	Chord, in	β (deg)
0.1500	5.5816	36.32
0.2000	5.6889	35.84
0.3000	5.8021	34.56
0.4000	5.7940	32.78
0.5000	5.6695	30.51
0.7000	5.0208	24.87
0.7500	4.7548	23.38
0.8000	4.4369	21.94
0.9000	3.6171	19.36
1.0000	2.4971	17.56

Table 8 Static thrust of 1C160/DTM7557 predicted by ROTOR II

RPM	Thrust, lb	P_{req}, Hp
500	31	1.29
1000	124	10.32
1500	278.99	34.82
2000	495.97	82.54
2500	774.96	161.21

This thrust prediction was used as a reference to determine the minimum thrust required for the model. The propulsion parameters predicted by ROTOR II such as RPM, thrust and power were scaled with a scale factor of 1/3 based on the scaling laws developed. It was found that the model would required minimum 28.7 lb static thrust at 4330RPM (see **Table 9**).

$$RPM_{model} = 1.732\ RPM_{172P}$$
$$Thrust_{model} = 0.037\ Thrust_{172P}$$
$$Power_{model} = 0.021\ Power_{172P}$$

Table 9 Scaling laws applied to the prototype to obtain the thrust, power and RPM required by the model

RPM_{172P}	$Thrust_{172P}$, lbs	$Power_{172P}$, Hp	RPM_{model}	$Thrust_{model}$ lbs	$Power_{model}$ Hp
500	31	1.29	866	1.148148	0.02758
1000	124	10.32	1732	4.592593	0.220642
1500	278.99	34.82	2598	10.33296	0.744452
2000	495.97	82.54	3464	18.36926	1.764705
2500	774.96	161.21	4330	28.70222	3.44667

To verify the scale factor that was used to compute the thrust required for the model, the 1C160/DTM7557 was scaled down geometrically using the one-third-scale factor. The following table is the geometry of the one-third-scaled 1C160/DTM7557. For ease of labeling, the one-third-scaled 1C160/DTM7557 was named "model".

Table 10 Inputs of 1/3-scaled 1C160/DTM7557 for ROTOR II

r/R	chord, in	ch/3, in	β (deg)
0.1500	5.5816	1.8605	36.32
0.2000	5.6889	1.8963	35.84
0.3000	5.8021	1.9340	34.56
0.4000	5.7940	1.9313	32.78
0.5000	5.6695	1.8898	30.51
0.7000	5.0208	1.6736	24.87
0.7500	4.7548	1.5849	23.38
0.8000	4.4369	1.4790	21.94
0.9000	3.6171	1.2057	19.36
1.0000	2.4971	0.8324	17.56

The predictions determined from ROTOR II were in good agreement with the scaling law in both thrust and power required. Due to the Reynolds number of a model airplane propeller being much lower than a typical general aviation aircraft propeller (3 million for GA, 50,000 for model), drag corrections are necessary. **Table 11** gives the results predicted by ROTOR II compared against those of the scaling laws.

Table 11 Comparison of thrust, and power required using ROTOR II and the scaling laws

RPM	$T_{rotor\ II}$	T_{scaled}	%diff
866	1.148	1.148148	0.012903
1732	4.592	4.592593	0.012903
2598	10.33	10.33296	0.028675
3464	18.37	18.36926	-0.00403
4330	28.7	28.70222	0.007742

Predicted power required without Reynold's number correction

RPM	$P_{rotor\ II}$	P_{scaled}	%diff
866	0.0276	0.02758	-0.07252
1732	0.2206	0.220642	0.019035
2598	0.7445	0.74445	-0.00672
3464	1.765	1.7647	-0.017
4330	3.45	3.44667	-0.09661

Predicted power required without Reynold's number correction

RPM	$P_{rotor\ II}$	P_{scaled}	%diff
866	0.0375	0.02758	-35.9681
1732	0.29	0.220642	-31.4346
2598	0.946	0.74445	-27.0737
3464	2.177	1.7647	-23.3637
4330	4.14	3.44667	-20.1159

7.0 Flight performance analysis

At this point, the performance of the tested propellers looks promising based upon the experimental data collected in these tests. All the tested propellers were able to produce 40 lb of static thrust or more. Also, the maximum static thrust produced by each tested propellers were about 15 lb higher than the static thrust required found by scaling law. In this section of the research was to investigate the flight performance of each tested propellers, and to determine if the tested propellers were able to meet the flight performance requirement for the model.

An efficiency chart for 1C160/DTM7557M1 propeller was obtained from the Embry-Riddle Aeronautical University In-Flight Laboratory data. Again, to ensure the validity of the ROTOR II program, the propeller efficiencies predicted by ROTOR II were compared with the efficiencies of In-Flight lab data. In **Figure 20**, the general trend in the efficiency of the propeller rotating at 2500RPM had good agreement with the efficiency of full size prop. On the other hand, the efficiency curve of the model is slightly lower. This is due to fact that the predicted power absorbed by the propeller had a Reynolds number drag adjustment. As a result of this drag adjustment, the model required more power to drive the propeller and meant lower efficiency. Data that are used to plot the following graph are attached in **Appendix E**.

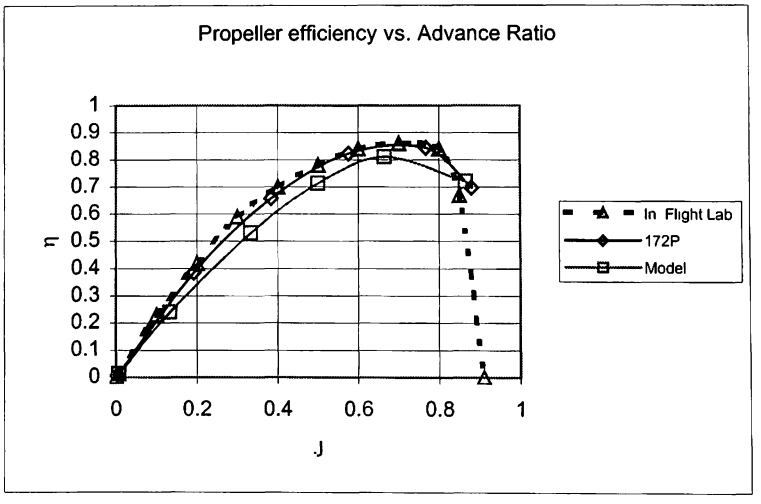

Figure 20 Comparison of the efficiency curve predicted by ROTOR II with In-Flight Laboratory data

The Q100XL was not specifically designed and manufactured to match the scaled engine performance of the Lycoming O-320-D2J installed on the Cessna 172P. Therefore the scaled power required for the tested propellers were not taken into account in the propeller in-flight performance analysis. The following graphs is the flight performance prediction of the scaled propeller, Bolly G28 x 10, Bolly G26 x 12 and Syntec Vari-Pitch (Pitch setting 10) at 4330RPM standard sea level conditions. From **Figure 21**, it clearly shows that all the tested propellers were not able to deliver the thrust required for the model to cruise in the designed cruise speed (67kts, 113ft/s) at 4330RPM. Also, from the plotted efficiency curves, the tested propellers had the best efficiency at low advance ratio which is about 0.45 (**see Figure 22**). In contrast, the scaled propeller has the best efficiency at advance ratio of 0.75. This suggests that the tested propellers were not designed for cruise performance rather for climb performance. That is, their pitch is too low to scale the performance of a real aircraft.

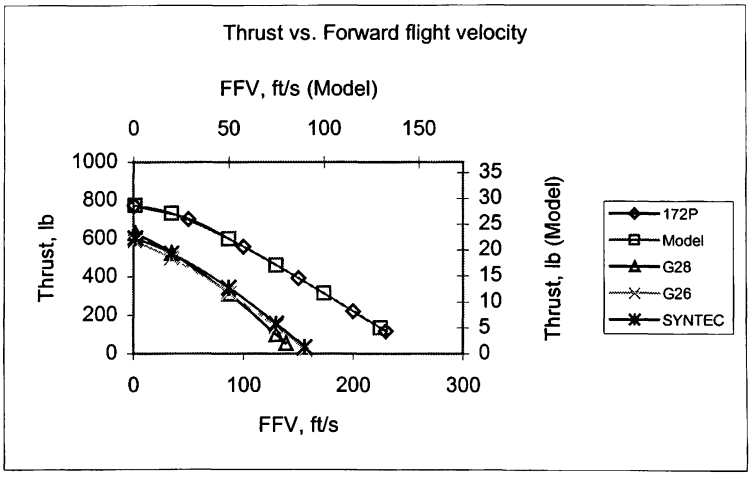

Figure 21 Thrust versus forward flight velocity of Cessna 172P @ 2500RPM; 1/3-scaled Cessna 172P, Bolly G28x10, Bolly G26x12, Syntec Vari-Pitch Prop (Classic blade @ pitch setting 10) @ 4330RPM

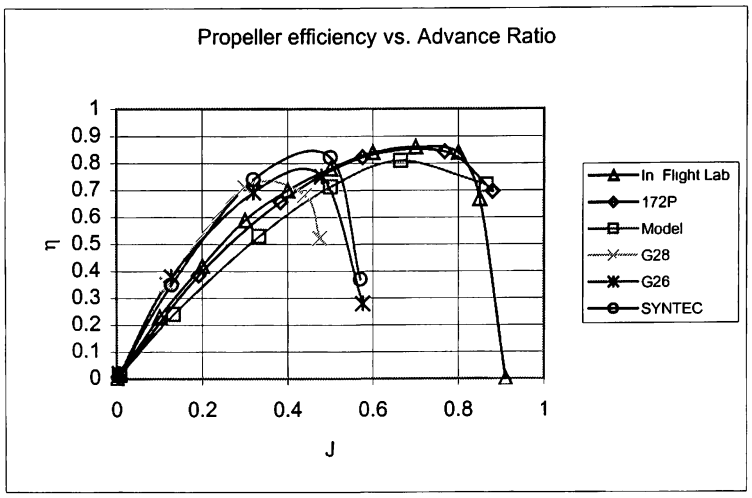

Figure 22 Propeller efficiency versus advance ratio for Cessna 172P @ 2500RPM; 1/3-scaled Cessna 172P, Bolly G28x10, Bolly G26x12, Syntec Vari-Pitch Prop (Classic blade @ pitch setting 10) @ 4330RPM

Further flight performance analysis was done to fully understand the capability of each tested propeller. From the static thrust test data, all propellers performed well above 4330RPM. Therefore, several analyses were performed on the tested propellers with higher propeller rotational speed. With higher RPM, the flight performance of the tested propellers did improve (see **Figure 23**).

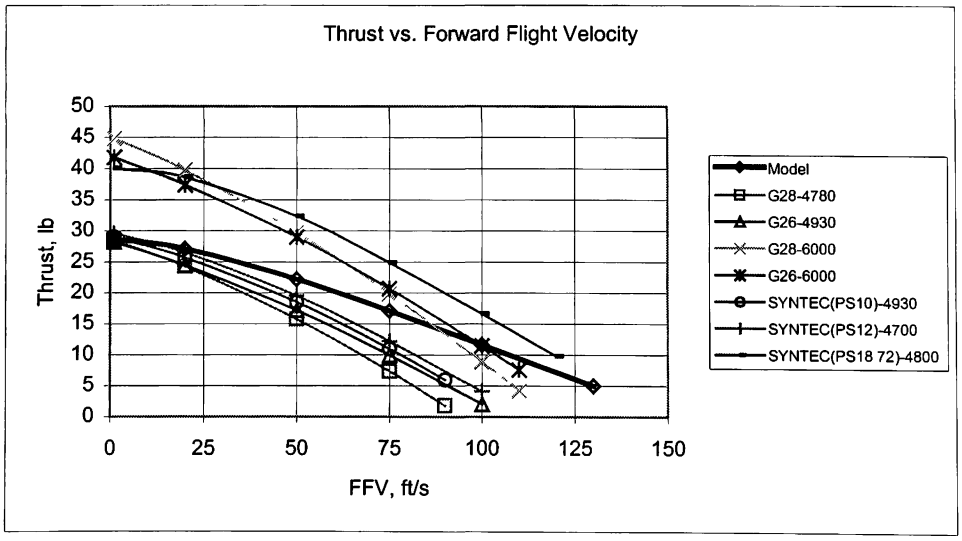

Figure 23 Thrust versus forward flight velocity of 1/3-scaled Cessna 172P, Bolly G28x10, Bolly G26x12, Syntec Vari-Pitch Prop (Classic blade @ pitch setting 10)

For the propeller efficiency, there was no improvement with the increase propeller rotational speed (see **Figure 24**). These appear to suggest the propellers tested may be intended for use as high performance climb propeller. Also, the low blade angle distribution suggested that these propellers were not designed to fly at a high cruise velocity. In addition, all the tested propellers were off the shelf products that were designed for general use and not for application to scientifically scaled model airplanes. It was not a surprise that these propellers were limited in meeting the flight envelope of the model.

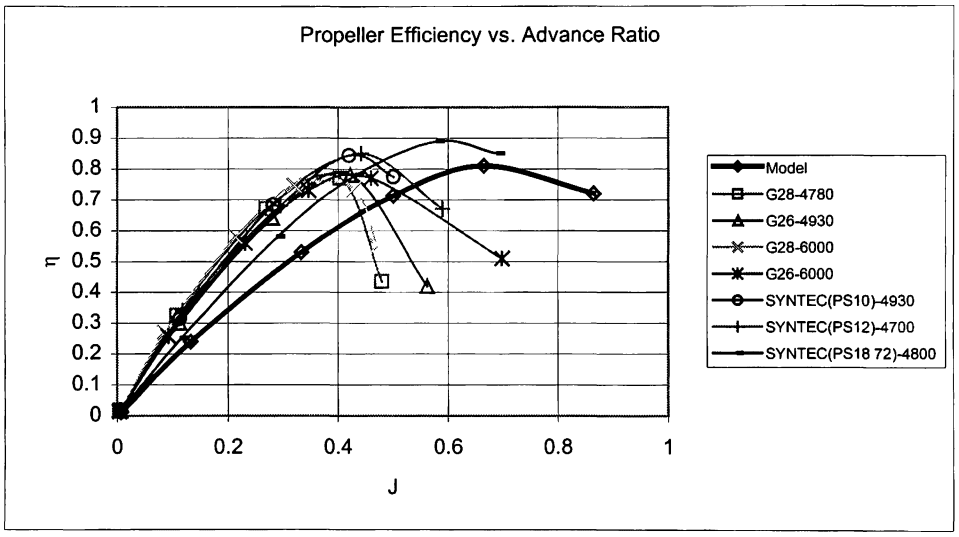

Figure 24 Propeller efficiency versus advance ratio of 1/3-scaled Cessna 172P, Bolly G28x10, Bolly G26x12, Syntec Vari-Pitch Prop (Classic blade @ pitch setting 10)

From the flight performance analyses, the results indicated that a custom made propeller may be needed. Based on the ROTOR II predictions, the scaled down version of the 1C160/DTM7557 was able to meet the flight performance required by the 1/3-scaled model airplane. This propeller can be custom manufactured with ease using the CNC milling machine (Computer numerical control milling machine) under the supervision of Aerospace Engineering Department. An analysis was also done on the power required to drive this propeller. The propeller required 4.62HP at 4500RPM whereas the Quatra Aerrow could only deliver 3-HP at this engine RPM (see **Figure 25**).

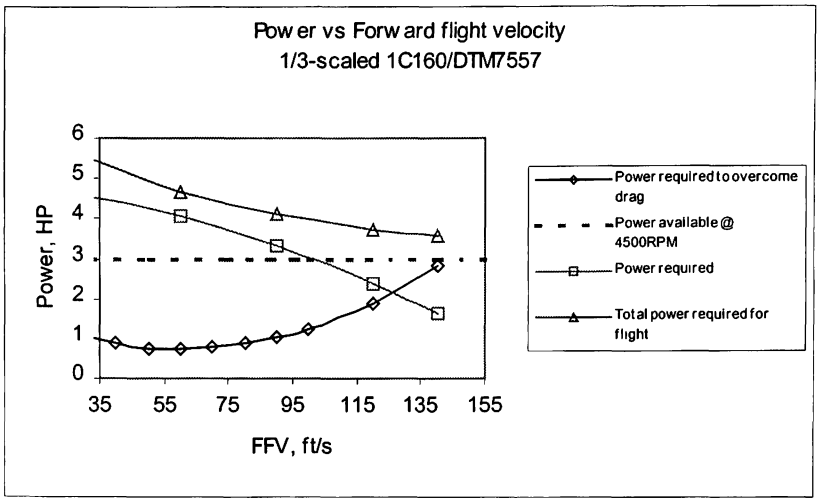

Figure 25 Power required to drive the 1/3-scaled 1C160/DTM7557 propeller

Once again, this suggests a different type of power plant may be necessary for the model. Through some research on two-cycle model aircraft engine, it was found that most giant scale model engine manufacturers design these engines to deliver a maximum power output between 8000 - 12000RPM. Apparently there was no engine readily available capable to deliver the power required by the model.

Before fully committing to a design of a new propeller and acquiring another engine for the model airplane, additional flight performance analysis was done on the Bolly G26 x 12. Bolly G28 x 10 was not selected for this part of the analysis due to its diameter was 3 inch greater than the scaled prop, and low pitch angle. Syntec Vari-Pitch was not analyzed simply due to the fact that the propeller will not be used on the flight test model for safety reasons. From these additional analyses, the propeller was found to be able to deliver the thrust required by the model in cruise condition at 6500RPM (**see Figure 26**). It was shown that the engine was capable of driving the Bolly G26 x 12 at 6200RPM experimentally.

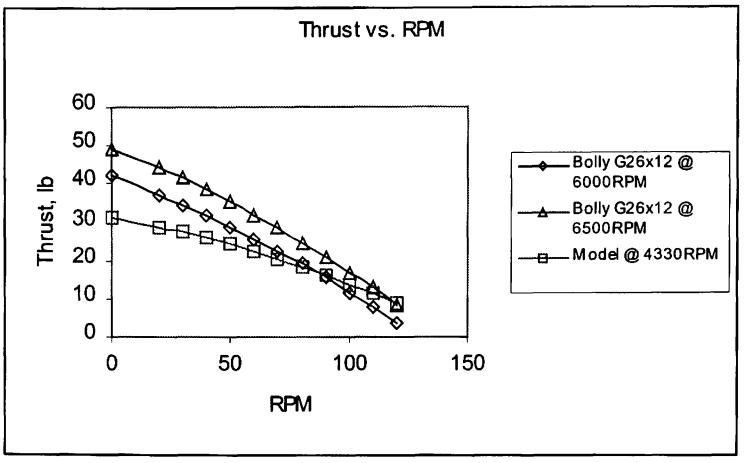

Figure 26 Thrust versus forward flight velocity of 1/3-scaled Cessna 172P, and Bolly G26 x 12

In the earlier discussion, all the propellers tested had the best propeller efficiency at advance ratio approximately 0.45. Again, due to the nature of the engine operated in high RPM, and the low blade angle of the propeller, the advance ratio was much lower than that of the ideal one found for the model airplane. Since the 1/3-scaled model airplane was not designed to investigate propeller efficiency, similar propeller efficiency as the full-scaled counterpart can be neglected. A flight performance chart of Bolly G26 x 12 was generated based on ROTOR II predictions. This chart will be used to select the correct engine operating points to get the required scaled thrust for the flight test model at different pre-determined flight conditions.

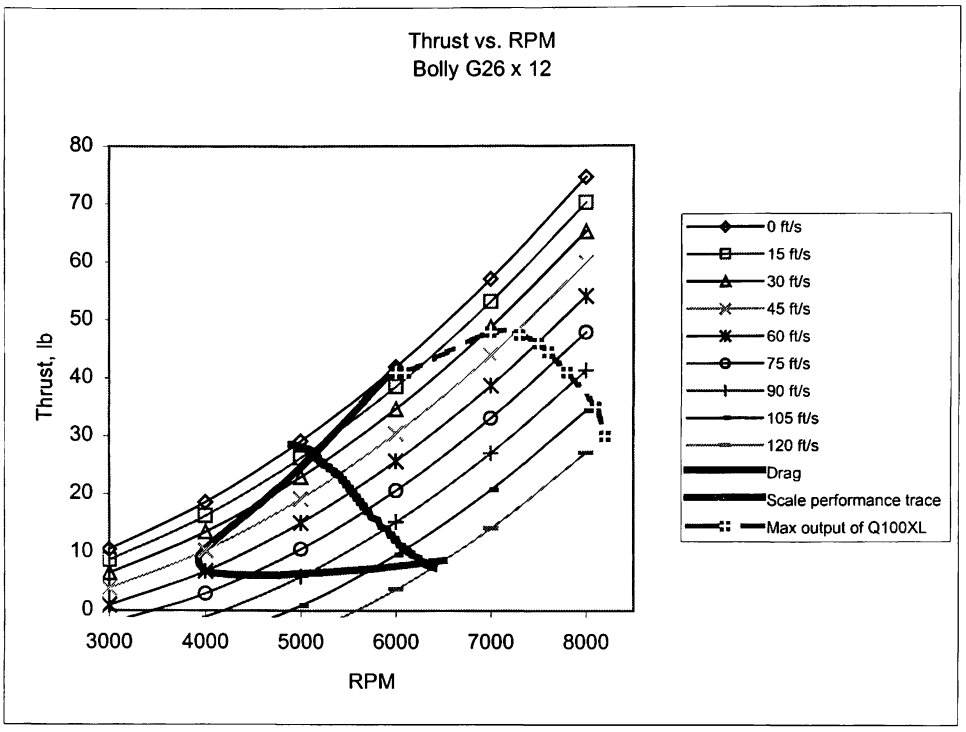

Figure 27 Flight performance envelope of Bolly G26 x 12

From **Figure 27**, the predicted thrust of Bolly G26 x 12 versus RPM was plotted at different forward flight velocity; the dotted line plotted on the graph was the drag of the model at different forward flight velocity; the plotted solid curve was the scale performance trace of the 1C160/DTM7557; the dotted curve with solid square marker was the maximum operating engine RPM at different forward flight velocity based on the data provided by Quatra Aerrow. As mentioned earlier, this chart was plotted for selecting correct engine operating points for the flight test model at different flight conditions. For instance, to fly at any desired forward speed, the pilot must operate the engine so as to produce propeller thrust equal to airplane drag. This family of curves will show the pilot what engine RPM should be used to accomplish that. The fact that the engine / propeller RPM is not scaled is unimportant because noise characteristic (dependant on propeller tip speed) are not being measured and not the focus of this research.

8.0 Conclusions

Several important findings were discovered in this research. First, the vibration induced by the engine was found to be far more extreme and severe than originally anticipated. As a result of this discovery, a separate investigation to attenuate vibrations is in progress. Secondly, a few problems were discovered while conducting the static thrust engine tests. For instance, the structural integrity of the muffler assembly was found to be unacceptable. The muffler assembly fell apart after a total of five hours running time on the engine. In addition, the ground adjustable pitch propeller proved to be unsafe for flight with the C172 model. After only three hours running time on the ground, the propeller flung a blade during a test. With these incidents on records, the possibility of a propeller failure, and the muffler disassembly in-flight may have been prevented. Lastly, as a result of these series static thrust tests and flight performance analysis done with the data from the tested propellers, it is concluded that Bolly G26 x 10 is able to meet the flight performance required of the model.

9.0 Recommendations

The irregular response throttle was significantly improved since the servo was relocated and mounts directly to the engine. There is still some improvement needed with respect to the throttle control mechanism before the engine is reinstalled back on the C172 model. All the OEM bellcranks should be replaced with custom bell-crank made out of a stiffer material such as aluminum. The change in the size and shape of the bell-crank is not necessary. By replacing these bellcranks, the throttle response will be more precise even if it operates in a severe vibration environment.

Reference

1. 1986 Skyhawk Information Manual, Cessna Aircraft Company.

2. Archer R.D., Saarlas M., An introduction to Aerospace Propulsion, Prentice Hall, Upper Saddle River, New Jersey 07458, 1996.

3. Baker W.E., Dodge F.T., Similarity Methods in Engineering Dynamics – Theory and Practice of Scale Modeling, Elsever Science Publishing Inc. 655 Avenue of the Americas, New York, N.Y. 10010, USA.

4. Borst H.V., Design and Analysis of Propellers for Low Reynolds Number Application to Mini-RPV's, Society of Automotive Engineers (Aerospace meeting), November 14-17 1977.

5. Dommasch D.O., Sherby S.S, Connolly T.F., Aircraft Aerodynamics, Third edition, Pitman Aeronautical Publications, 1957.

6. Gessow A., Myers G.C., Aerodynamics of The Helicopter, Frederick Ungar Publishing Co., 250 Park Avenue South, New York, N.Y. 10003, 1978.

7. Hall S., Dynamic Modeling, Sport Aviation, July 1987.

8. Hinton M.J., Eastlake C.N., The Construction and Flight Testing of a Scaled, Remotely-Piloted, Flight-Test Vehicle, 99 ASEE Conference, Session 2206.

9. Munk M.M., Warner E.P., Comparing the Performance of Geometrically Similar Airplanes, National Advisory Committee for Aeronautics, No.190, April 1924.

10. Professor C.N. Eastlake, ROTOR program, Embry-Riddle Aeronautical University - Department of Aerospace Engineering.

11. Professor C.N. Eastlake, Experimental Aerodynamics and Wind Tunnels – AE309 Lecture Notes and Laboratory Manual, Fifth edition, December 1999.

12. Raymer D.P., Aircraft Design: A Conceptual Approach, American Institute of Aeronautics and Aestronautics.

13. Seddon J., Basic Helicopter Aerodynamics, Blackwell Science, 1990.

14. Stewart J., Calculus, Brooks/Cole Publishing Company, Pacific Grove, California.

15. Stout E.G., Development of High-Speed Water-Based Aircraft, Journal of the Aeronautical Sciences, August 1950.

16. Stout E.G., Development of Precision Ratio-Controlled Dynamically Similar Flying Models, Journal of the Aeronautical Sciences, July 1946.

17. Taylor M., Holcomb J., Model for Test and Designing Homebuilt Aircraft, Sport Aviation, Jan 1987.

18. Woodward D.R., Zeck H., Spray Characteristic and Take-off and Landing Stability of Several Modifications of a 1/8-size Model of the PBN-1 Flying Boat – NACA Model 192, NACA WR L5030.

19. Zahm A. F., Theories of Flow Similitude, Aerodynamical laboratory, Bureau of Construction and Repair, U.S. Navy.

APPENDIX

Appendix A: Experimental data

The following equations were used to correct experimentally measured thrust to Standard sea-level conditions.

$$P = \rho RT$$

$$\rho_{test} = \frac{P_{NOAA}}{RT_{NOAA}}$$

$$\rho_{STD} = 0.002376 \frac{slug}{ft^3}$$

$$T_{adjusted} = T_{measured} \frac{\rho_{STD}}{\rho_{test}}$$

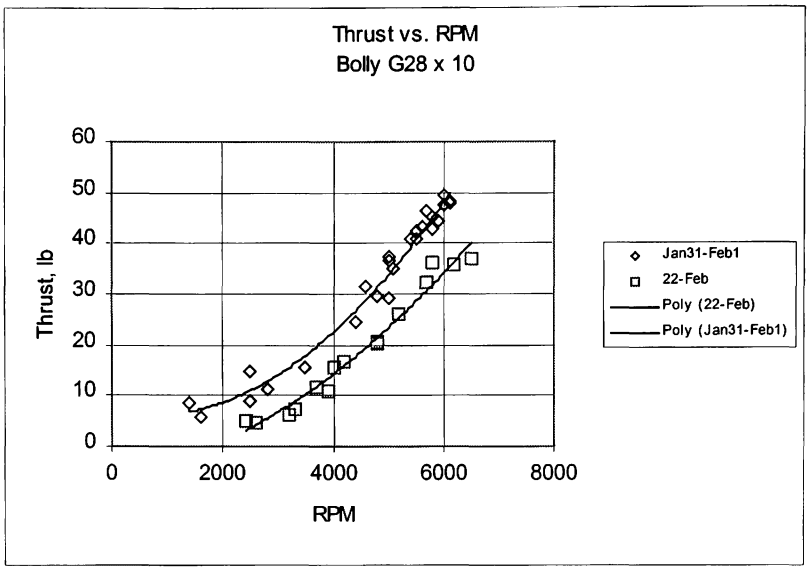

Figure 1A Experimental data of Bolly G28 x 10 with temperature and pressure corrected to STD conditions

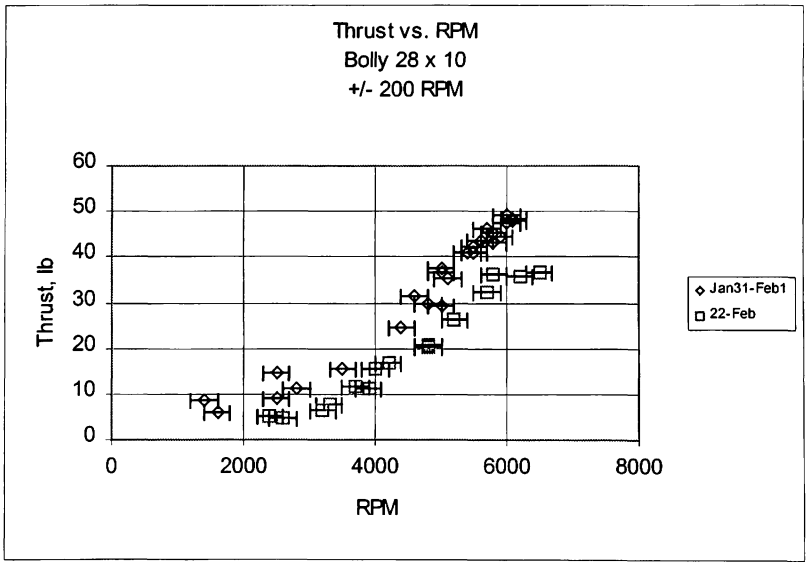

Figure 2A Experimental data of Bolly G28 x 10 with uncertainty introduced

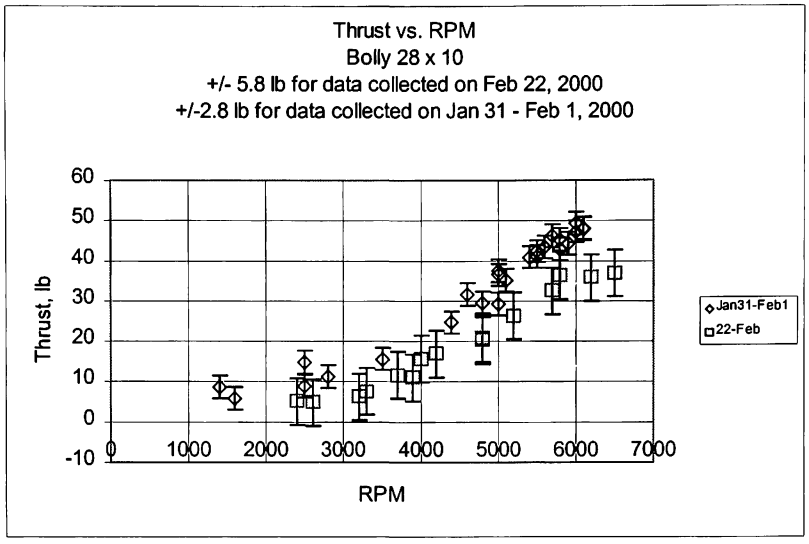

Figure 3A Experimental data of Bolly G28 x 10 with uncertainty introduced

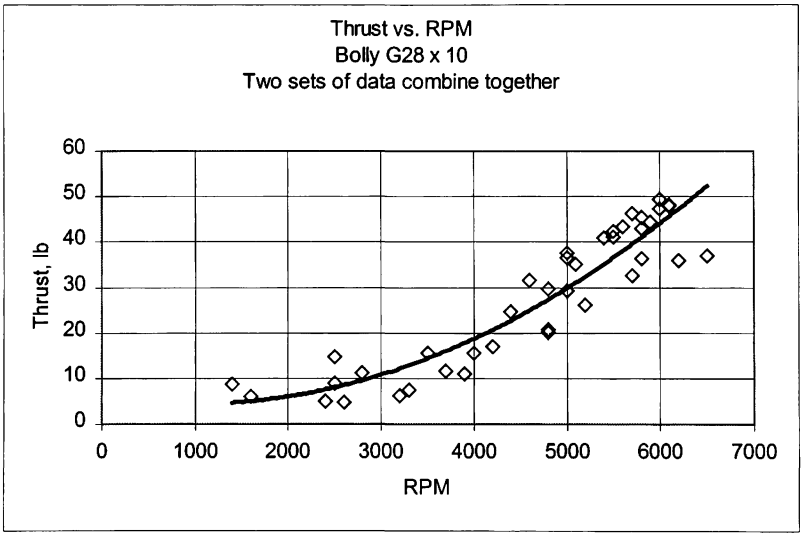

Figure 4A Second degree polynomial was used to curve fit the experimental data of Bolly G28 x 10

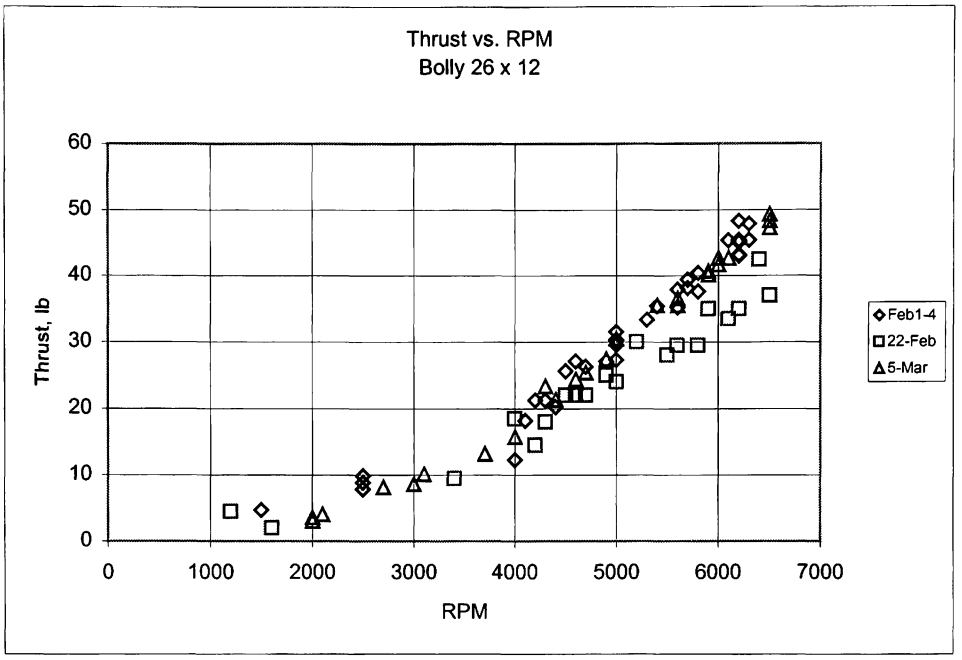

Figure 5A Experimental data of Bolly G26 x 12 with temperature and pressure corrected to STD conditions

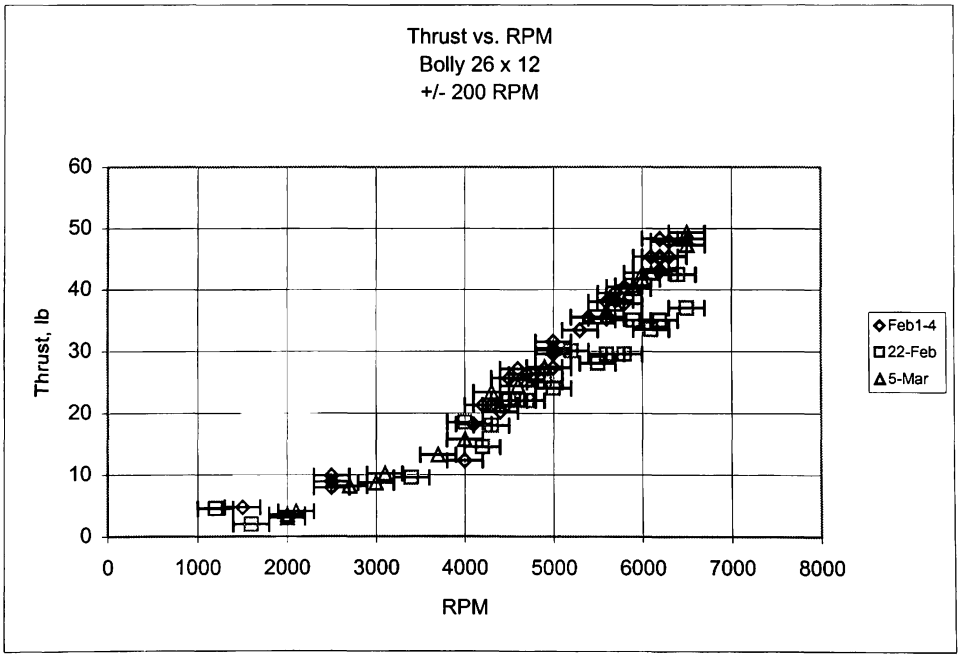

Figure 6A Experimental data of Bolly G26 x 12 with uncertainty introduced

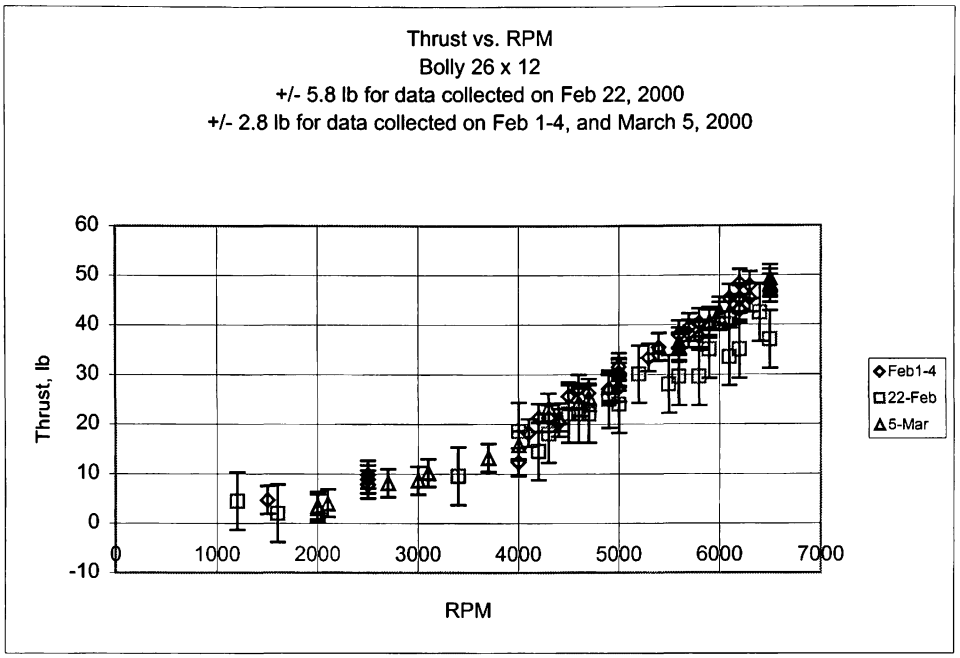

Figure 7A Experimental data of Bolly G26 x 12 with uncertainty introduced

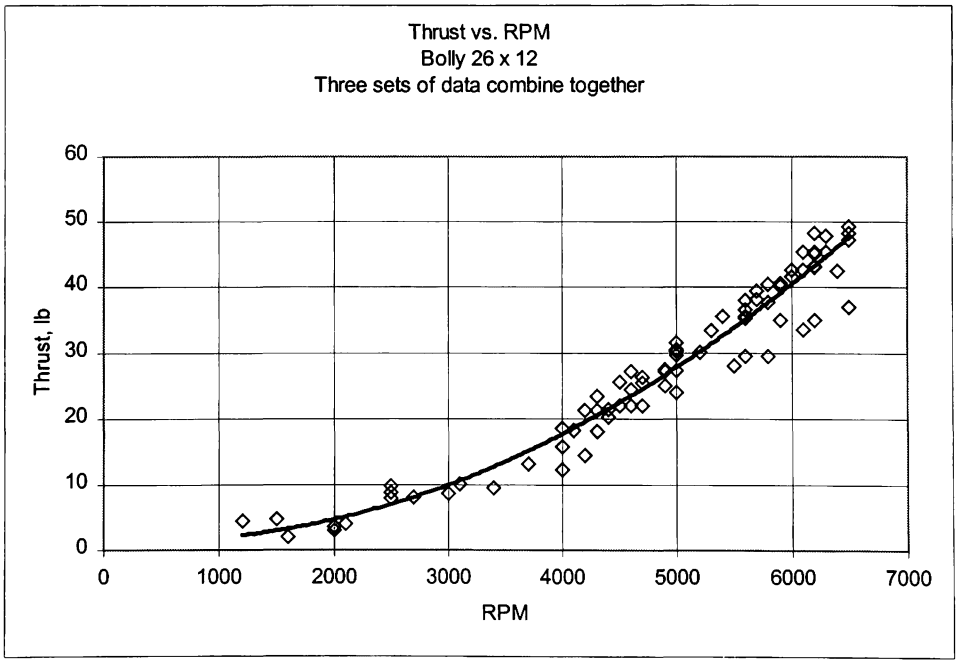

Figure 8A Second degree polynomial was used to curve fit the experimental data of Bolly G26 x 12

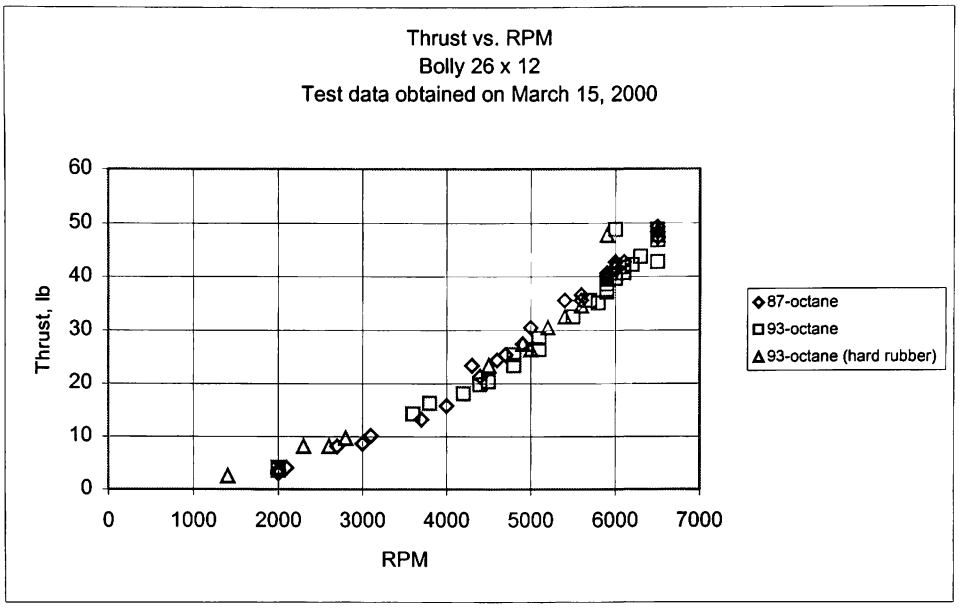

Figure 9A Experimental data of Bolly G26 x 12 with temperature and pressure corrected to STD conditions

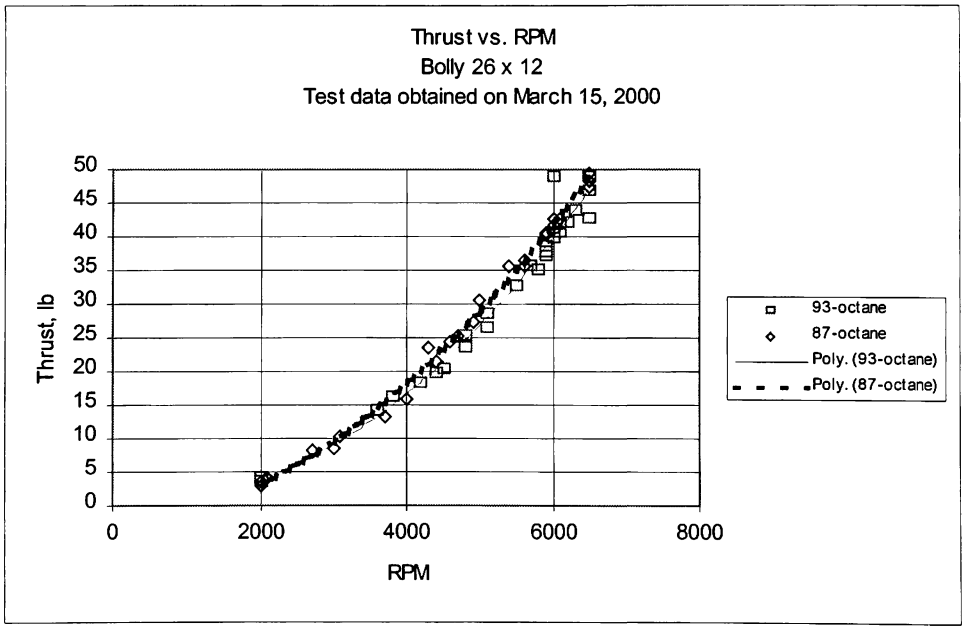

Figure 10A Investigate the effect of octane rating on engine performance with Bolly G26 x 12

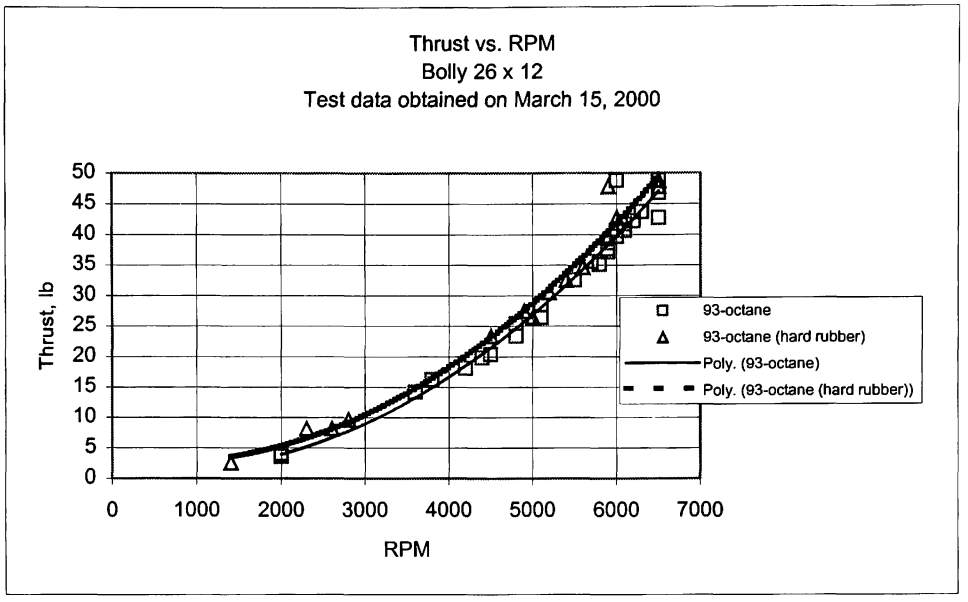

Figure 11A Investigate the effect of vibration damping material setup on the load scale reading with Bolly G26 x 12

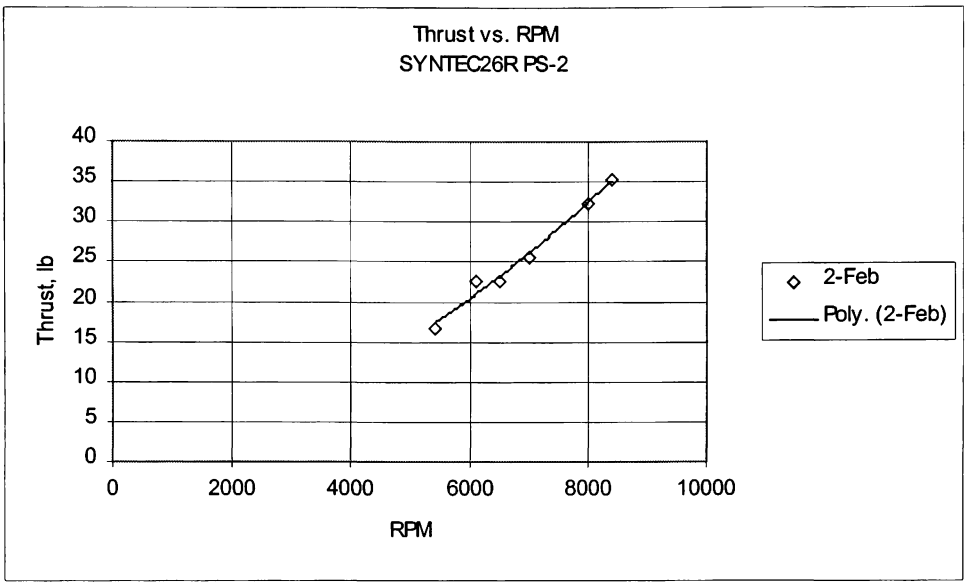

Figure 12A Experimental data of Syntec Vari-Pitch (26" classic blade, pitch setting-2) with temperature and pressure corrected to STD conditions

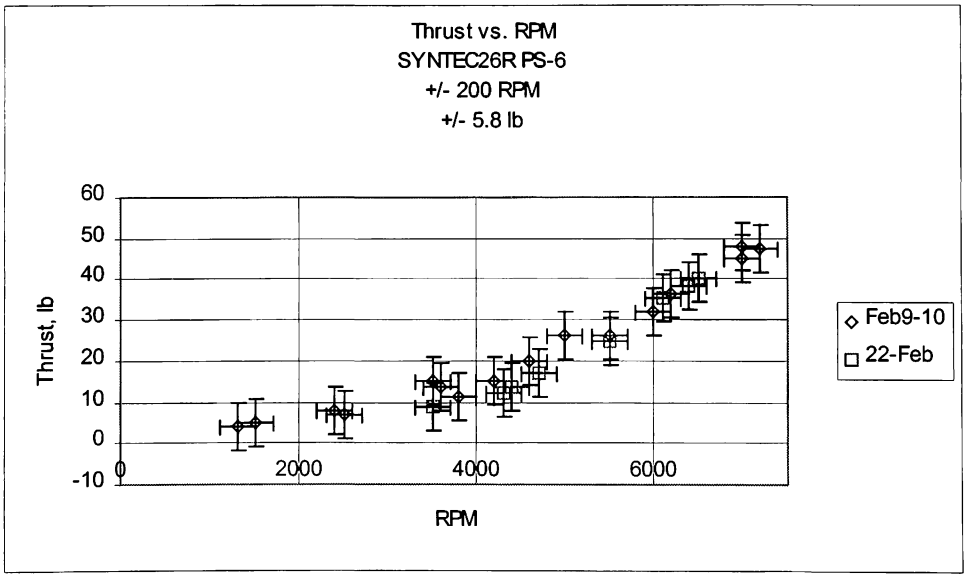

Figure 13A Experimental data of Syntec Vari-Pitch (26" classic blade, pitch setting-6) with uncertainty introduced

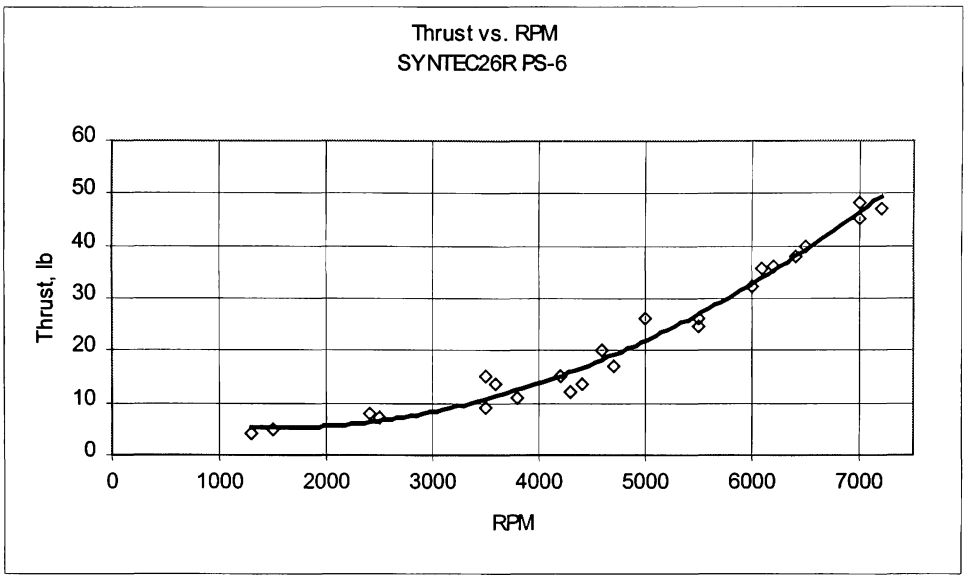

Figure 14A Second degree polynomial was used to curve fit the experimental data of Syntec Vari-Pitch (26" classic blade, pitch setting-6)

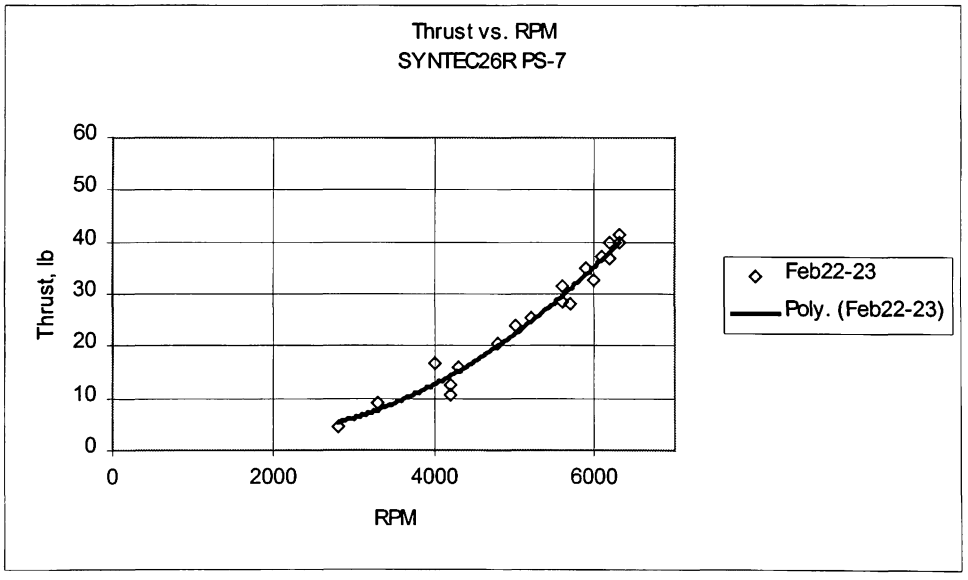

Figure 15A Experimental data of Syntec Vari-Pitch (26" classic blade, pitch setting-7) with temperature and pressure corrected to STD conditions

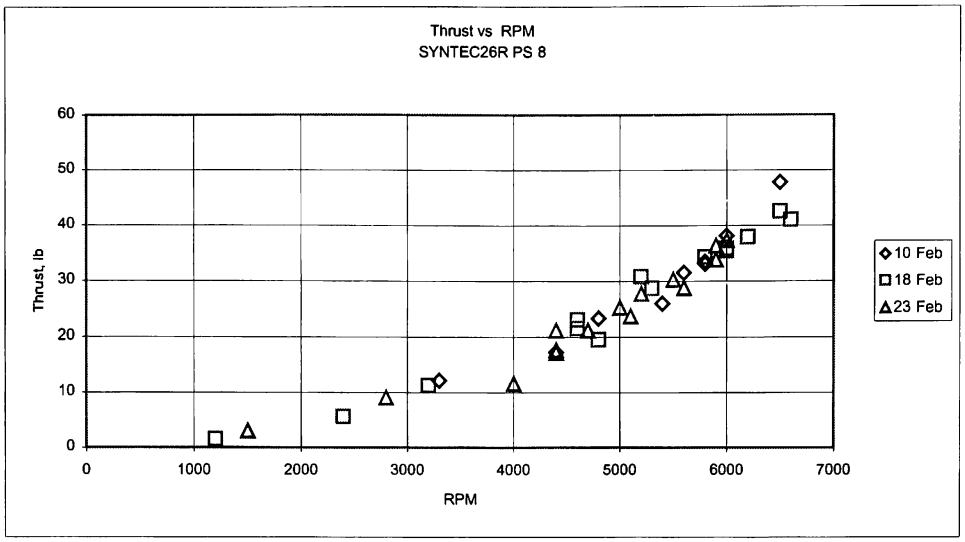

Figure 16A Experimental data of Syntec Vari-Pitch (26" classic blade, pitch setting-8) with temperature and pressure corrected to STD conditions

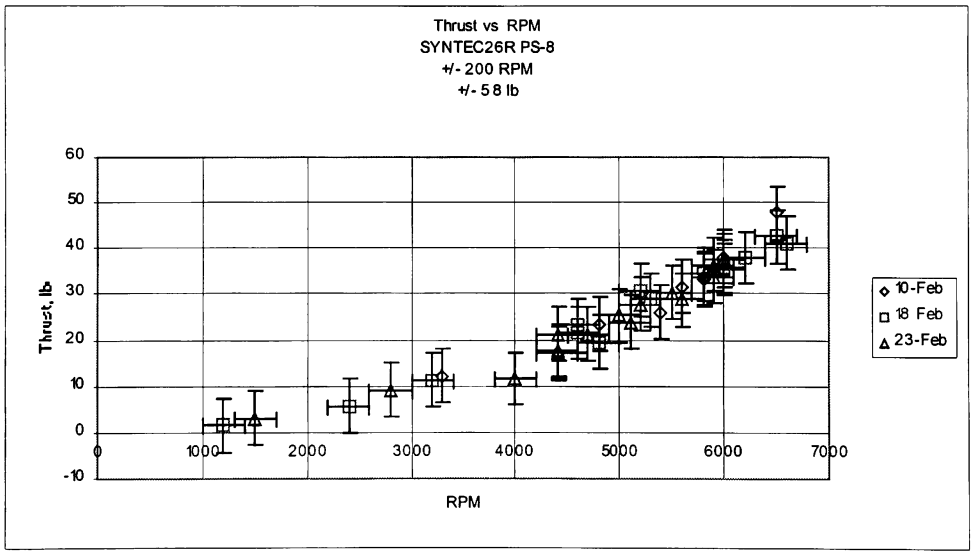

Figure 17A Experimental data of Syntec Vari-Pitch (26" classic blade, pitch setting-8) with uncertainty introduced

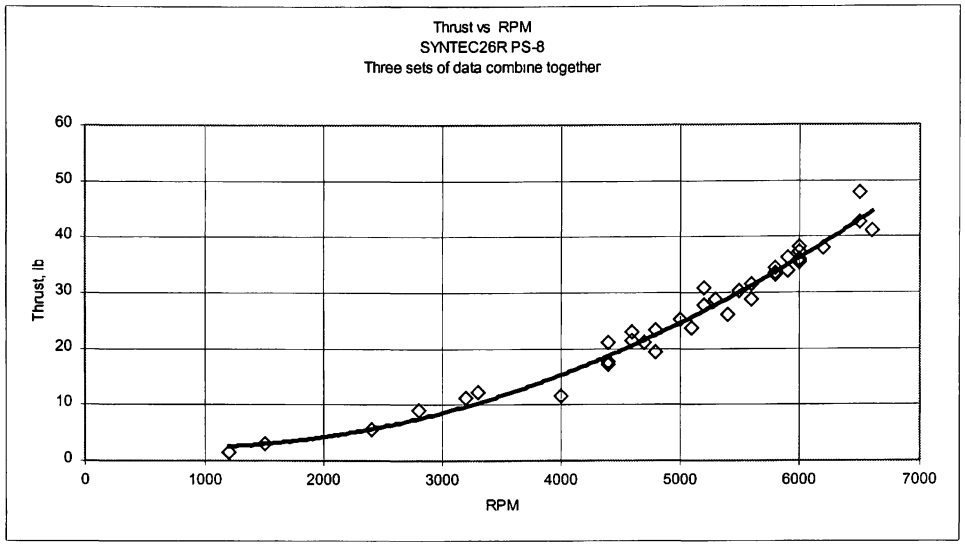

Figure 18A Second degree polynomial was used to curve fit the experimental data of Syntec Vari-Pitch (26" classic blade, pitch setting-8)

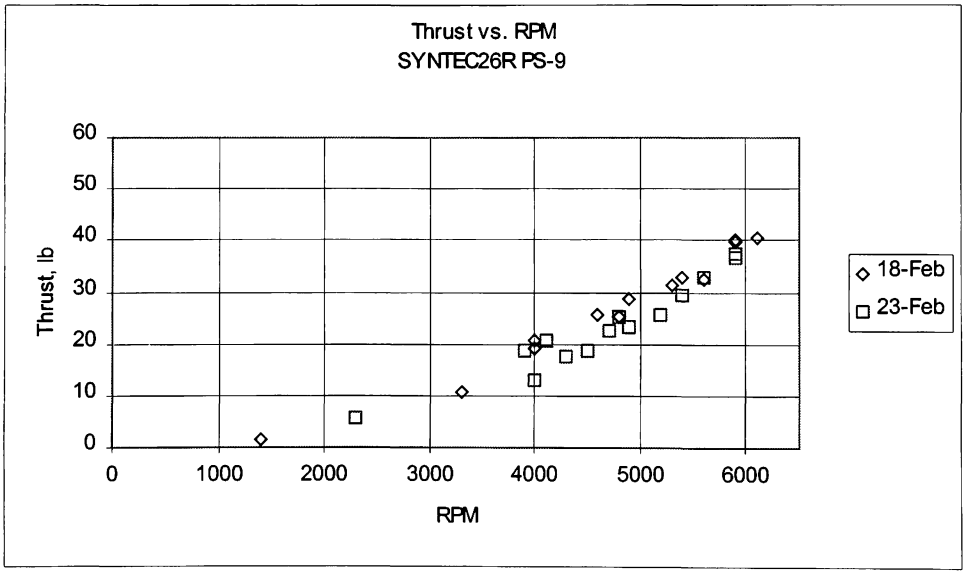

Figure 19A Experimental data of Syntec Vari-Pitch (26" classic blade, pitch setting-9) with temperature and pressure corrected to STD conditions

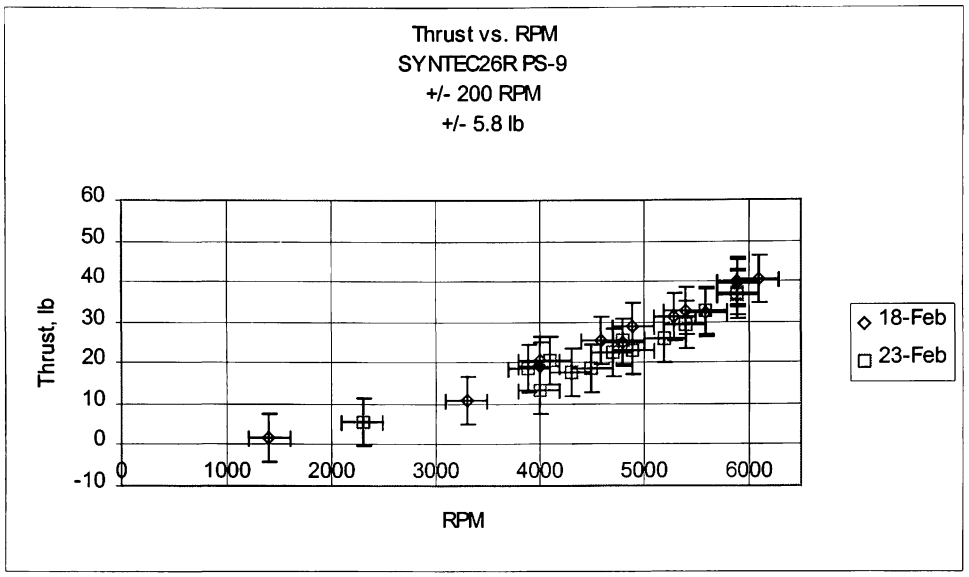

Figure 20A Experimental data of Syntec Vari-Pitch (26" classic blade, pitch setting-9) with uncertainty introduced

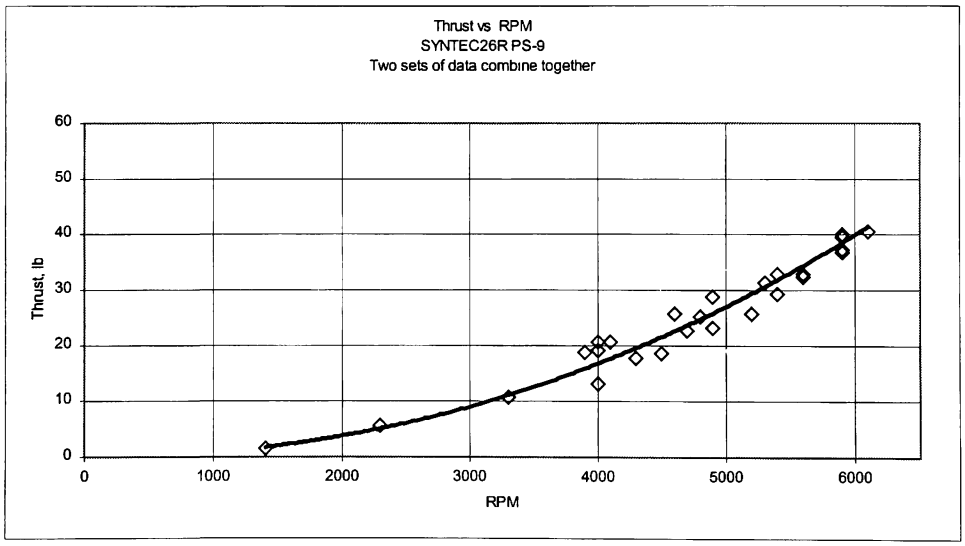

Figure 21A Second degree polynomial was used to curve fit the experimental data of Syntec Vari-Pitch (26" classic blade, pitch setting-9)

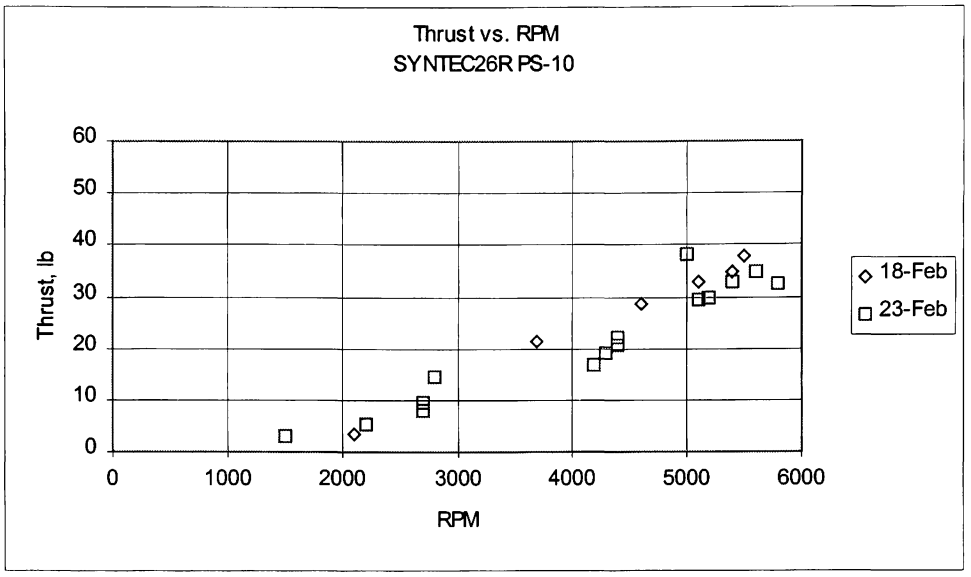

Figure 22A Experimental data of Syntec Vari-Pitch (26" classic blade, pitch setting-10) with temperature and pressure corrected to STD conditions

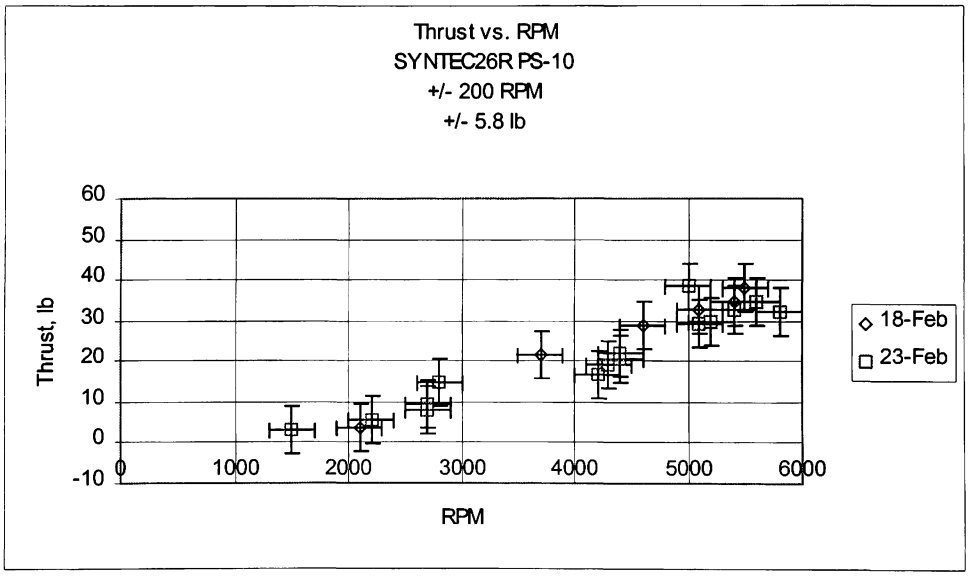

Figure 23A Experimental data of Syntec Vari-Pitch (26" classic blade, pitch setting-10) with uncertainty introduced

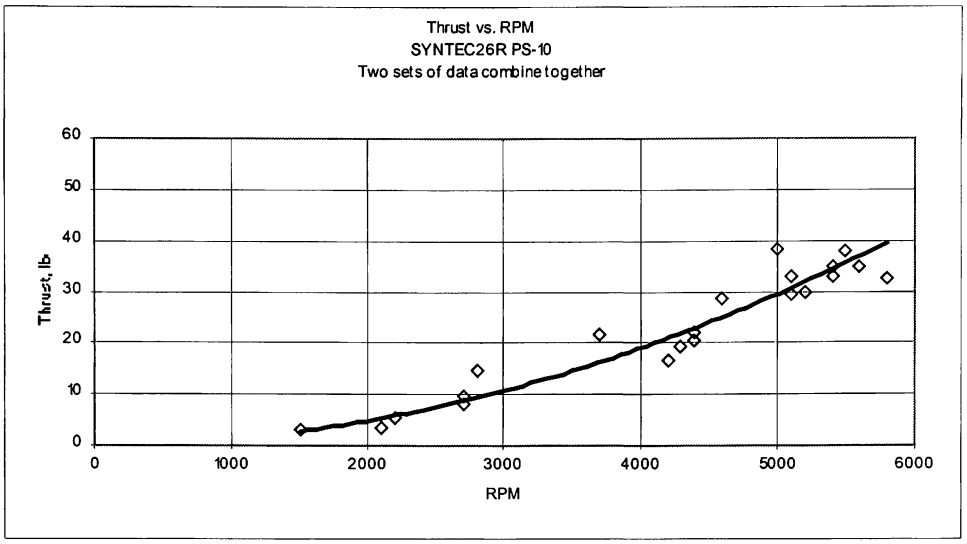

Figure 24A Second degree polynomial was used to curve fit the experimental data of Syntec Vari-Pitch (26" classic blade, pitch setting-10)

Appendix B: Sample calculation of Drag correction factor

Formula	ω:	$rpm*2\pi/60$
	Velocity:	$r/12*\omega$
	Re#:	Velocity*chord/12/v, v=0.00015723

Bolly Graphite Prop 28 x 10

						rpm	2000		rpm	4000	
						ω	209.333333		ω	418.666667	
r, in	chord, in	r/R	β	t, in	t/c	velocity	Re#	CF		Re#	CF
3	1.875	0.21428571	25.7562037	0.43307	0.23097067	52.3333333	52007.1445	2.25015093	104.666667	104014.289	1.95887016
5.5	2	0.39285714	17.9576031	0.354331	0.1771655	95.9444444	101702.86	1.96769425	191.888889	203405.721	1.71297734
8	1.9375	0.57142857	12.4144883	0.295276	0.15240052	139.555556	143308.576	1.83725659	279.111111	286617.152	1.59942476
11	1.5	0.78571429	8.16225566	0.216525	0.14435	191.888889	152554.291	1.81442644	383.777778	305108.581	1.57954996
14	0.375	1	5.85540061	0.059055	0.15748	244.222222	48540.0016	2.28141501	488.444444	97080.0031	1.98608712
							avg:	**2.03018864**		avg:	**1.76738187**

Bolly Graphite Prop 26 x 12

						rpm	2000		rpm	4000	
						ω	209.333333		ω	418.666667	
r, in	chord, in	r/R	β	t, in	t/c	velocity	Re#	CF		Re#	CF
2.5	1.75	0.19230769	27.2028944	0.43307	0.24746857	43.6111111	40450.0013	2.36614058	87.2222222	80900.0026	2.05984501
5	1.9375	0.38461538	19.6019646	0.354331	0.18288052	87.2222222	89567.86	2.0183376	174.444444	179135.72	1.75706494
7.5	1.875	0.57692308	15.46601	0.275591	0.14698187	130.833333	130017.861	1.87337037	261.666667	260035.723	1.63086363
10	1.5	0.76923077	11.536959	0.216535	0.14435667	174.444444	138685.719	1.84934485	348.888889	277371.437	1.6099482
13	0.375	1	9.20689622	0.07874	0.20997333	226.777778	45072.8586	2.31548105	453.555556	90145.7172	2.01574333
							avg:	**2.08453489**		avg:	**1.81469302**

Syntec Vari-pitch Prop - 26" classic blade

						rpm	2000		rpm	4000	
						ω	209.333333		ω	418.666667	
r, in	chord, in	r/R	β	t, in	t/c	velocity	Re#	CF		Re#	CF
2.833333	1.90533333	0.30769231	13.8865404	0.43307	0.22729356	49.4259259	49912.4765	2.26872798	98.8518519	99824.953	1.97504242
5.166667	1.93033333	0.5	7.18075578	0.314961	0.16316405	90.1296296	92211.1071	2.0066314	180.259259	184422.214	1.7468741
7.5	1.81166667	0.69230769	4.58856574	0.23622	0.13038822	130.833333	125626.147	1.88628905	261.666667	251252.294	1.64210999
9.833333	1.516	0.84615385	3.12677611	0.177165	0.11686346	171.537037	137828.949	1.85163833	343.074074	275657.898	1.61194479
12.16667	0.94333333	1	2.29244278	0.07874	0.08346996	212.240741	106115.121	1.95105178	424.481481	212230.242	1.69848923
							avg:	**1.99286771**		avg:	**1.73489211**

Appendix C: Comparing static thrust prediction between ROTOR and ROTOR II

Bolly G28 x 10

RPM	T_{Rotor}	$T_{rotor\ II}$
1000	1.2695	1.25
2000	5.08	5.01
3000	11.43	11.27
5000	31.74	31.3
6000	45.7	45.08

Bolly G26 x 12

RPM	T_{Rotor}	$T_{rotor\ II}$
1000	1.165	1.265
2000	4.66	4.66
3000	10.48	10.5
5000	29.12	29.16
6000	41.94	42

SYNTEC26R

RPM	PS-8R	PS-10R	PS-8R2	KPS-10R2
1000	1.042391	1.178611	1.0477	1.198
3000	9.381517	10.6075	9.43	10.78
5000	26.05977	29.46527	26.16	29.942
7000	51.07715	57.75192	51.34	58.69

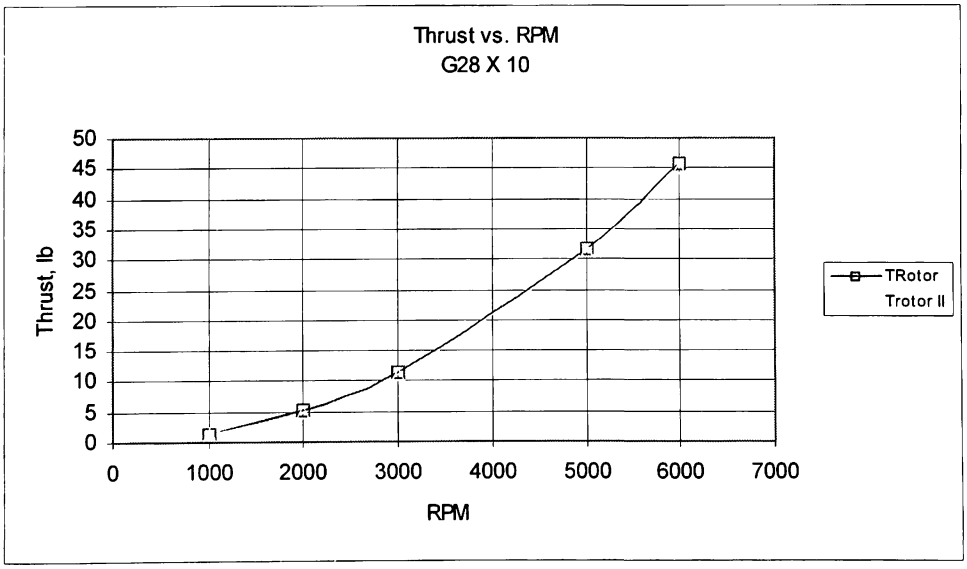

Figure 1C Comparing thrust prediction between Rotor and Rotor II of Bolly G28 x 10

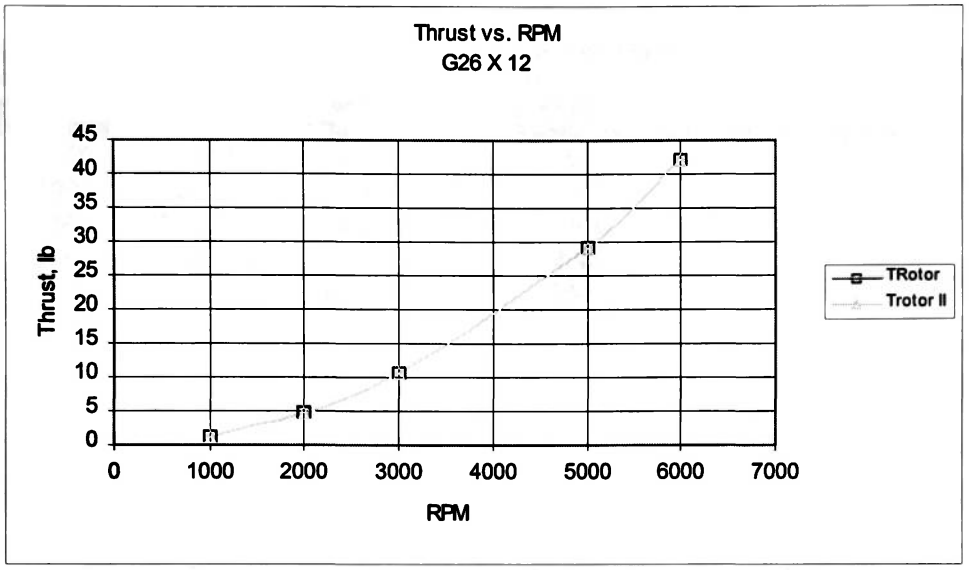

Figure 2C Comparing thrust prediction between Rotor and Rotor II of Bolly G26 x 12

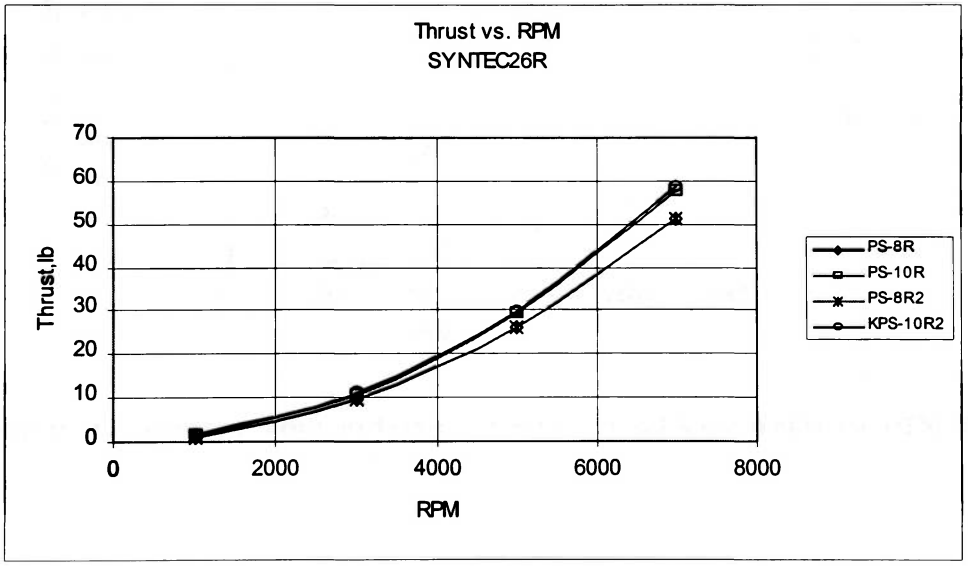

Figure 3C Comparing thrust prediction between Rotor and Rotor II of Syntec Vari-Pitch @ Pitch setting 8 & 10

Cessna (Rotor)
Static

RPM	Thrust, lb	P_{req}, Hp
500	31.01	1.305
1000	124.025	10.44
1500	279.056	35.22
2000	496.1	83.5
2500	775.15	163.1

Cessna (Rotor II)
Static

RPM	Thrust, lb	P_{req}, Hp
500	31	1.29
1000	124	10.32
1500	278.99	34.82
2000	495.97	82.54
2500	774.96	161.21

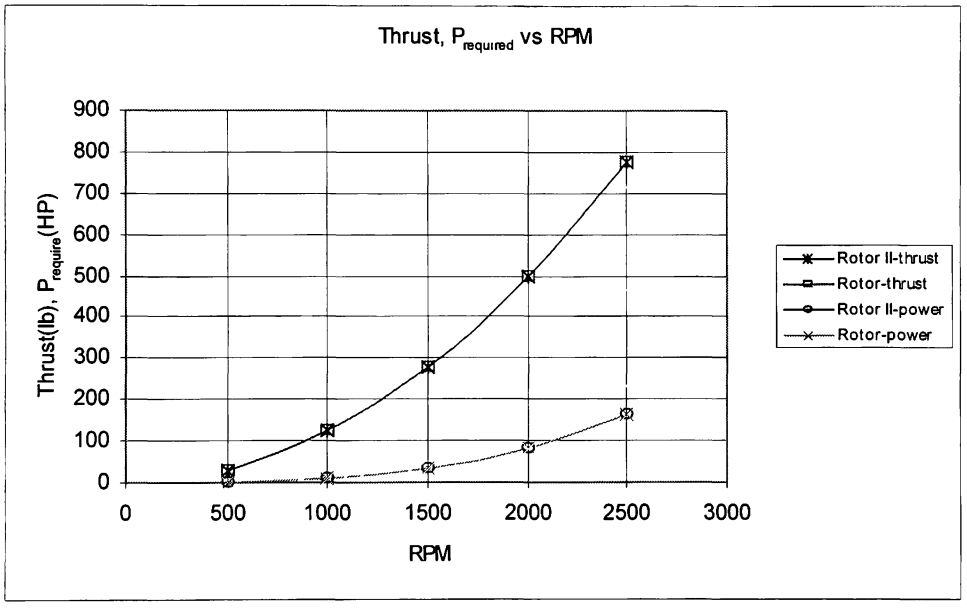

Figure 4C Comparing thrust prediction between Rotor and Rotor II of 1C160/DTM7557

Appendix D: Static performance predicted by ROTOR II

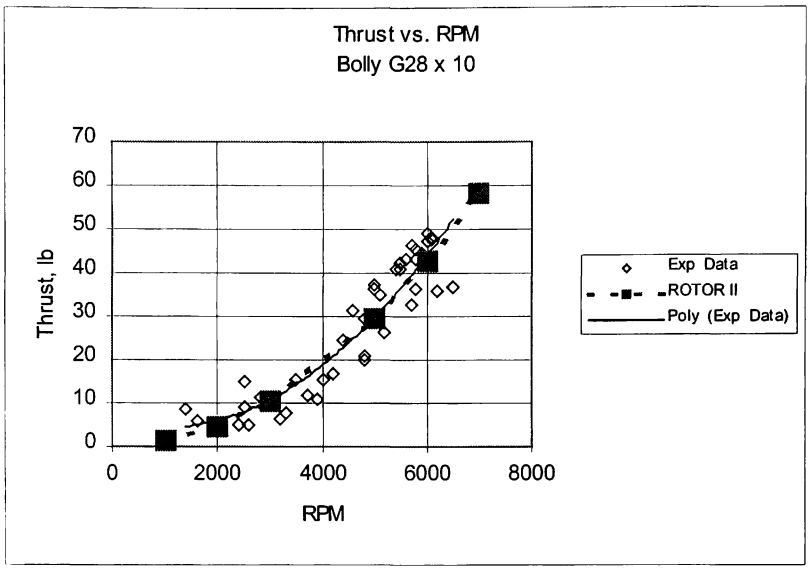

Figure 1D Experimental data compare with thrust prediction by Rotor II of Bolly G28 x 10

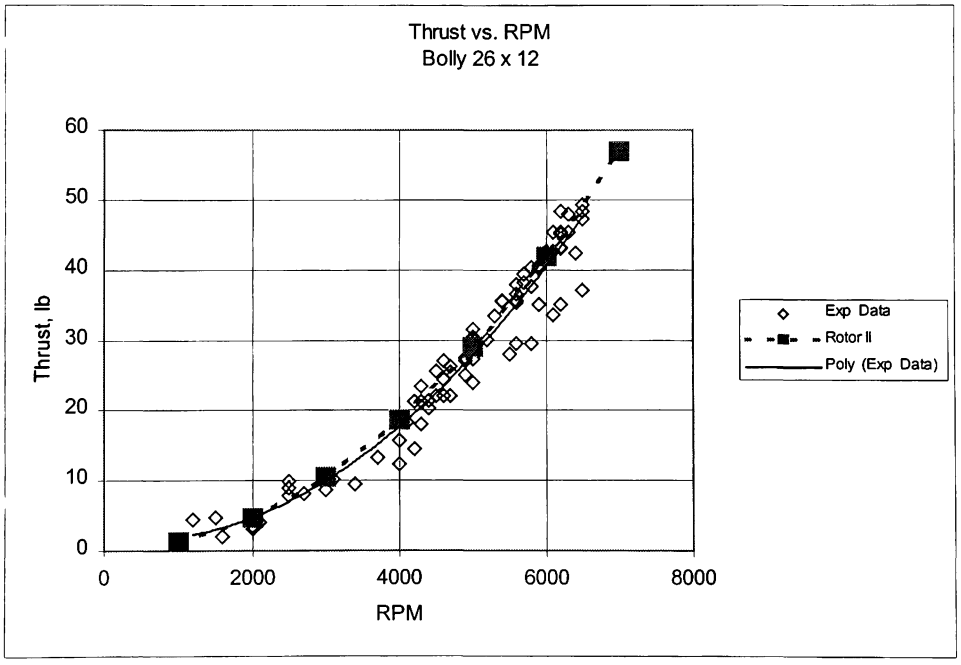

Figure 2D Experimental data compare with thrust predicted by Rotor II of Bolly G26 x 12

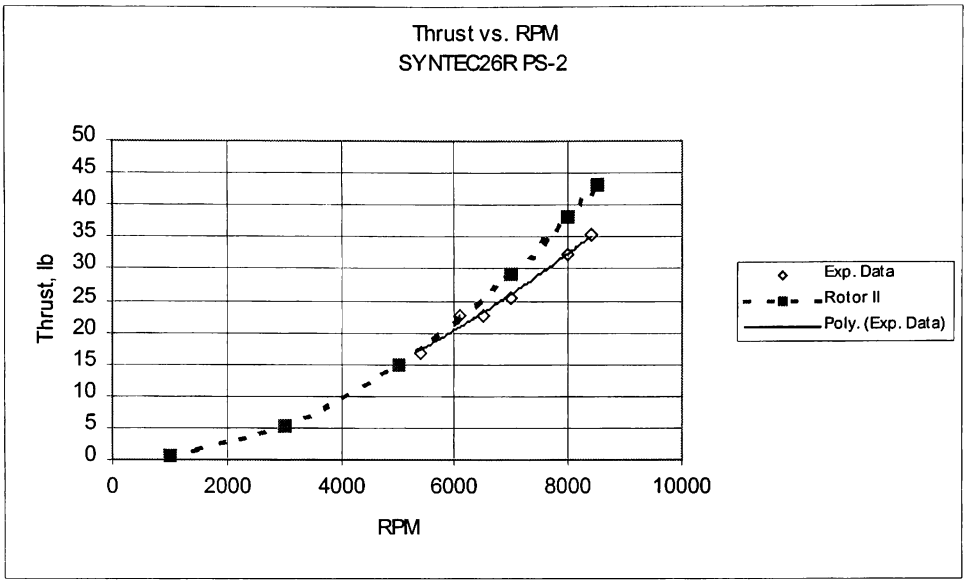

Figure 3D Experimental data compare with thrust predicted by Rotor II of Syntec Vari-Pitch

@ Pitch setting – 2

(The big deviation between the two curve was due to the propeller slipped during the test)

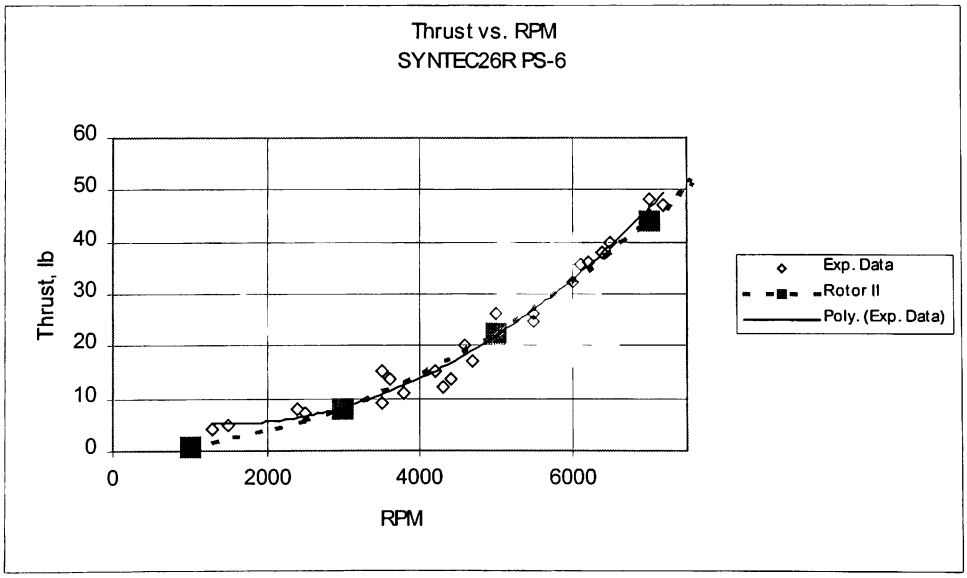

Figure 4D Experimental data compare with thrust predicted by Rotor II of Syntec Vari-Pitch

@ Pitch setting - 6

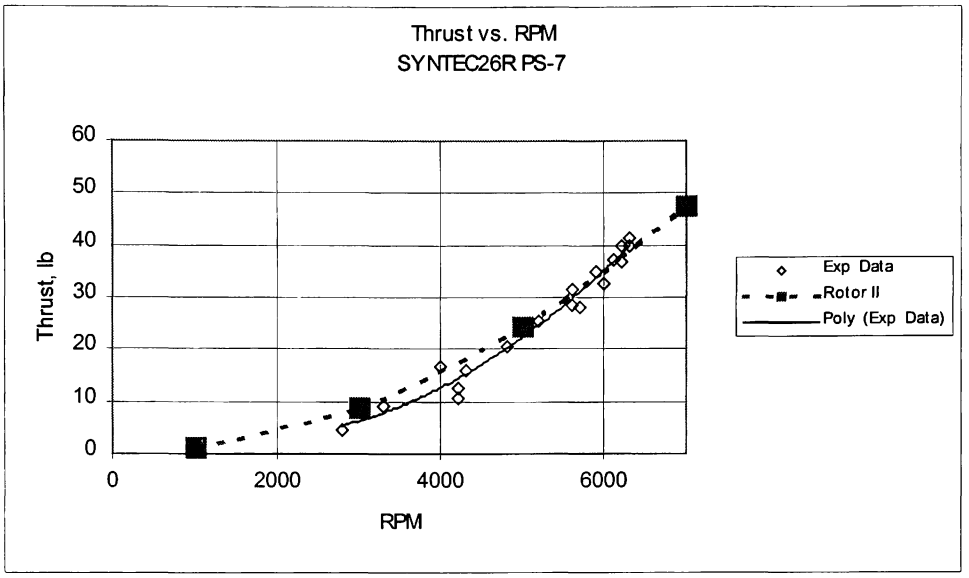

Figure 5D Experimental data compare with thrust predicted by Rotor II of Syntec Vari-Pitch

@ Pitch setting - 7

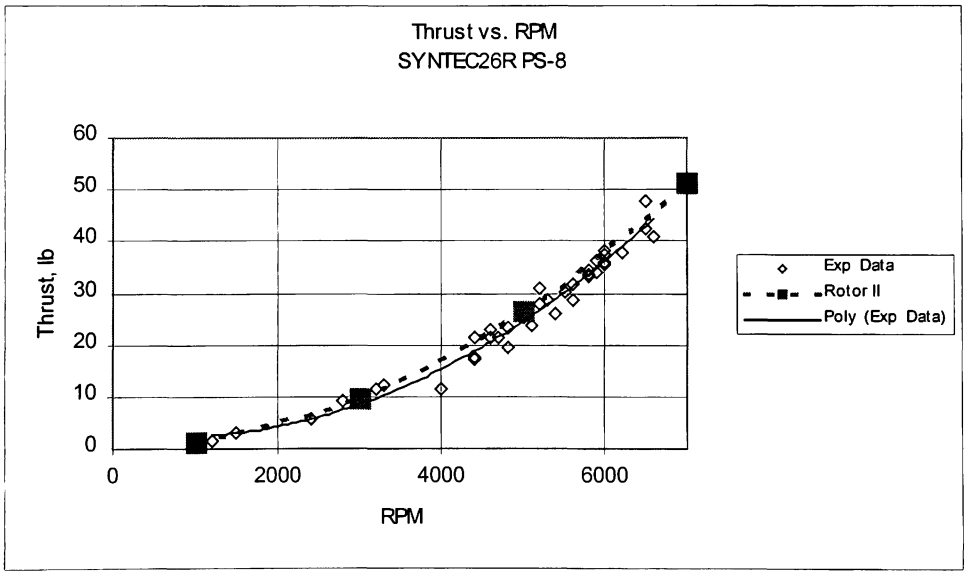

Figure 6D Experimental data compare with thrust predicted by Rotor II of Syntec Vari-Pitch

@ Pitch setting - 8

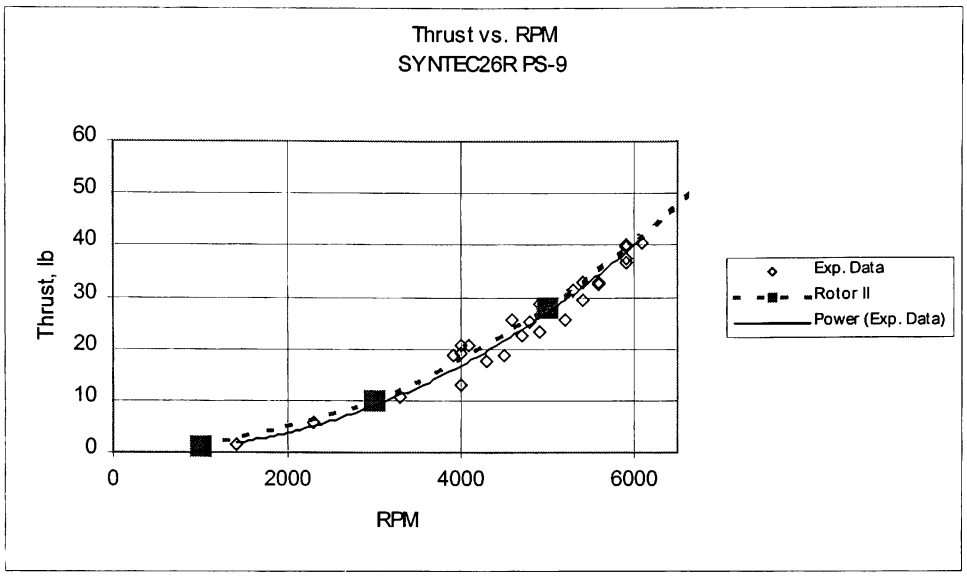

Figure 7D Experimental data compare with thrust predicted by Rotor II of Syntec Vari-Pitch @ Pitch setting - 9

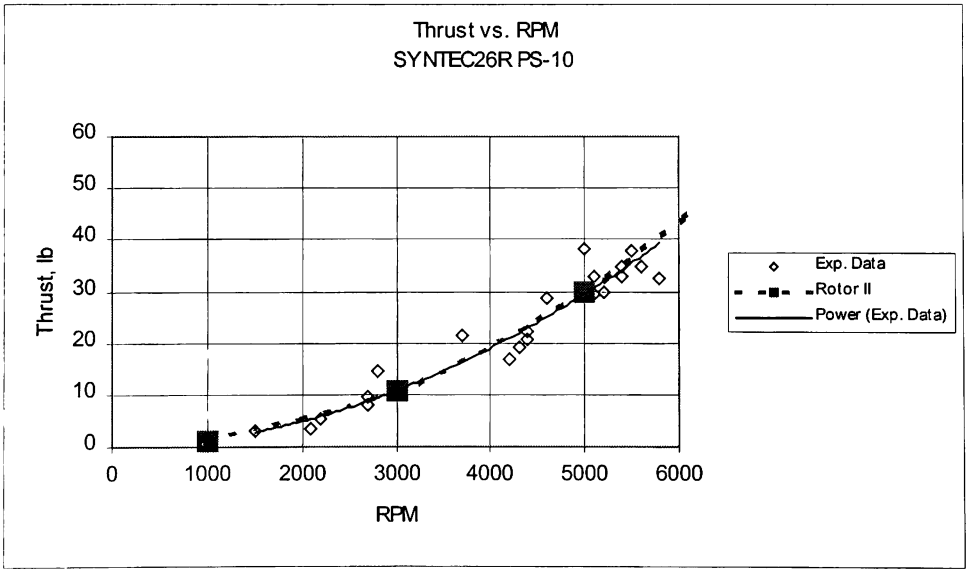

Figure 8D Experimental data compare with thrust predicted by Rotor II of Syntec Vari-Pitch @ Pitch setting - 10

Appendix E: Flight performance prediction of ROTOR II

172P **2500RPM**

FFV, ft/s	Thrust, lb	P_{req}, Hp	J	η
1	774.11	161.36	0.00384	0.008723
50	702.84	165.5	0.192	0.386
100	558.33	154.2	0.384	0.658
150	394.55	130.82	0.576	0.823
200	222.11	95.73	0.768	0.844
230	118.19	70.93	0.88	0.697

1/3 172P **4330RPM**

FFV, ft/s	Thrust, lb	P_{req}, Hp	J	η
1	28.64	4.14	0.0067	0.0126
20	27.1	4.11	0.133	0.24
50	22.2	3.78	0.333	0.53
75	17.11	3.27	0.5	0.713
100	11.67	2.61	0.665	0.81
130	4.99	1.64	0.865	0.72

Bolly G28 x 10 **4330RPM**

FFV, ft/s	Thrust, lb	P_{req}, Hp	J	η
1	23.31	2.15	0.0059	0.0197
20	19.455	2	0.1188	0.35
50	11.59	1.48	0.3	0.711
75	3.68	0.73	0.44	0.684
80	1.99	0.55	0.475	0.524

Bolly G26 x 12 **4330RPM**

FFV, ft/s	Thrust, lb	P_{req}, Hp	J	η
1	21.73	2.12	0.0064	0.0187
20	18.42	1.98	0.128	0.38
50	11.8	1.55	0.32	0.693
75	5.2	0.94	0.48	0.752
90	0.932	0.55	0.576	0.28

Syntec Vari-Pitch @ PS - 10 **4330RPM**

FFV, ft/s	Thrust, lb	P_{req}, Hp	J	η
1	22.33	2.154	0.0064	0.019
20	19.386	2.01	0.128	0.35
50	12.77	1.57	0.32	0.74
75	5.822	0.96	0.5	0.823
90	1.313	0.58	0.57	0.37

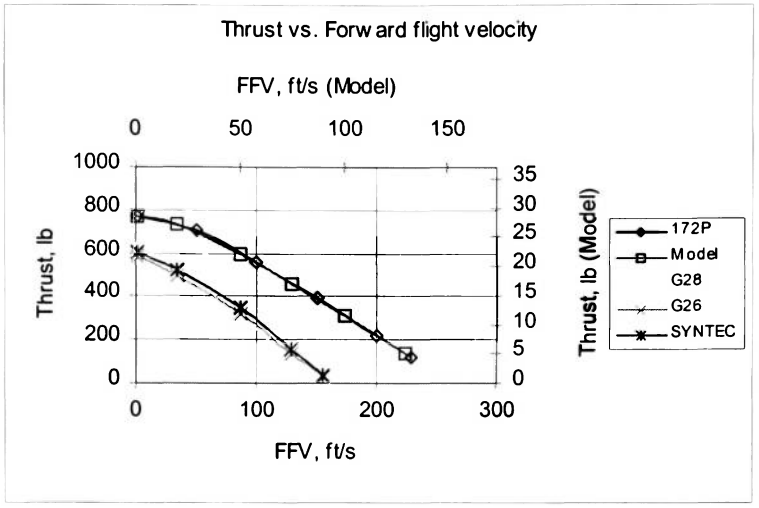

Figure 1E Flight performance predicted by Rotor II

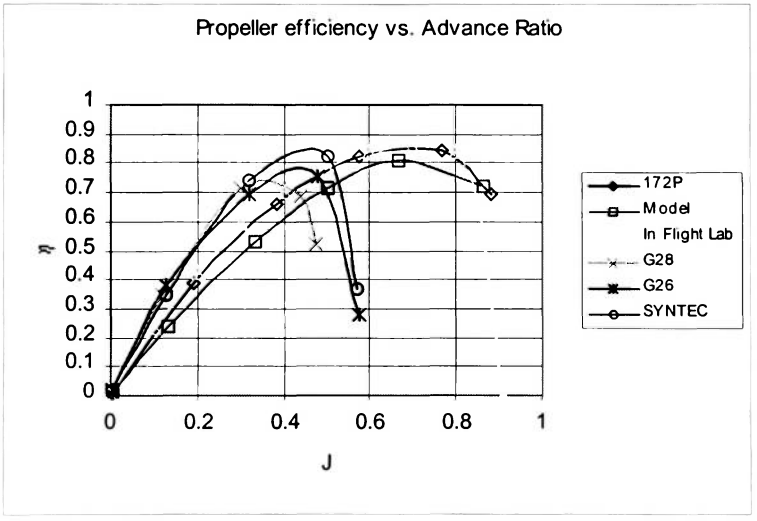

Figure 2E Propeller efficiency chart predicted by Rotor II

1/3 172P **4330RPM**

FFV, ft/s	Thrust, lb	P_{req}, Hp	J	η
1	28.64	4.14	0.0067	0.0126
20	27.1	4.11	0.133	0.24
50	22.2	3.78	0.333	0.53
75	17.11	3.27	0.5	0.713
100	11.67	2.61	0.665	0.81
130	4.99	1.64	0.865	0.72

Bolly G28 x 10 **4780RPM**

FFV, ft/s	Thrust, lb	P_{req}, Hp	J	η
1	28.43	2.87	0.0054	0.018
20	24.25	2.7	0.1076	0.326
50	15.78	2.13	0.269	0.67
75	7.33	1.3	0.404	0.77
90	1.79	0.67	0.48	0.435

Bolly G26 x 12 **4930RPM**

FFV, ft/s	Thrust, lb	P_{req}, Hp	J	η
1	28.19	3.09	0.0056	0.017
20	24.48	2.94	0.1123	0.3
50	17.2	2.44	0.28	0.64
75	9.98	1.75	0.4213	0.78
100	2.02	0.88	0.562	0.42

Syntec Vari-Pitch @ PS-10 **4930RPM**

FFV, ft/s	Thrust, lb	P_{req}, Hp	J	η
1	28.97	3.14	0.0056	0.017
20	25.69	2.97	0.1123	0.3145
50	18.53	2.47	0.281	0.683
75	10.974	1.77	0.42	0.844
90	6	1.266	0.5	0.774

Bolly G28 x 10 **6000RPM**

FFV, ft/s	Thrust, lb	P_{req}, Hp	J	η
1	44.85	5.6	0.0043	0.0146
20	39.72	5.36	0.086	0.27
50	29.74	4.66	0.214	0.58
75	19.88	3.63	0.32	0.747
100	8.88	2.2	0.4286	0.733
110	4.22	1.53	0.471	0.55

Bolly G26 x 12 **6000RPM**

FFV, ft/s	Thrust, lb	P_{req}, Hp	J	η
1	41.8	5.49	0.0046	0.0138
20	37.37	5.29	0.0923	0.257
50	28.94	4.69	0.2308	0.56
75	20.68	3.85	0.346	0.73
100	11.5	2.71	0.46	0.77
110	7.63	2.19	0.698	0.51

Syntec Vari-Pitch @ PS-12 (theoretical) **4700RPM**

FFV, ft/s	Thrust, lb	P_{req}, Hp	J	η
1	29.563	3.26	0.006	0.0165
20	26.5	3.11	0.118	0.34
50	19.54	2.62	0.295	0.68
75	12.21	1.95	0.442	0.85
100	4.11	1.114	0.59	0.67

Syntec Vari-Pitch @ PS-18.72 (theoretical) **4800RPM**

FFV, ft/s	Thrust, lb	P_{req}, Hp	J	η
1	40.05	5.62	0.0058	0.013
20	38.61	5.53	0.1154	0.25
50	32.32	5.082	0.29	0.58
75	24.89	4.37	0.433	0.78
100	16.65	3.4	0.58	0.89
120	9.83	2.5	0.69	0.85

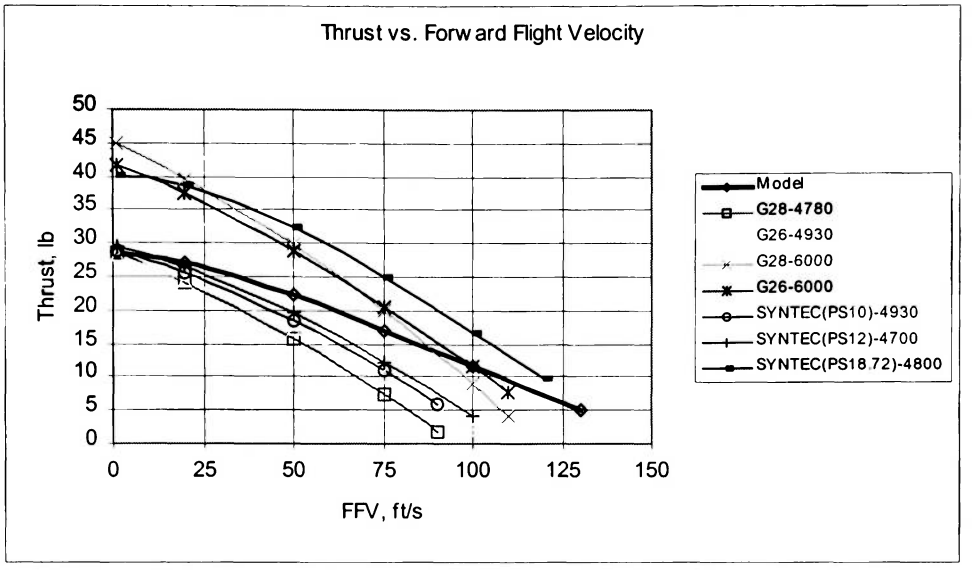

Figure 3E Flight performance predicted by Rotor II

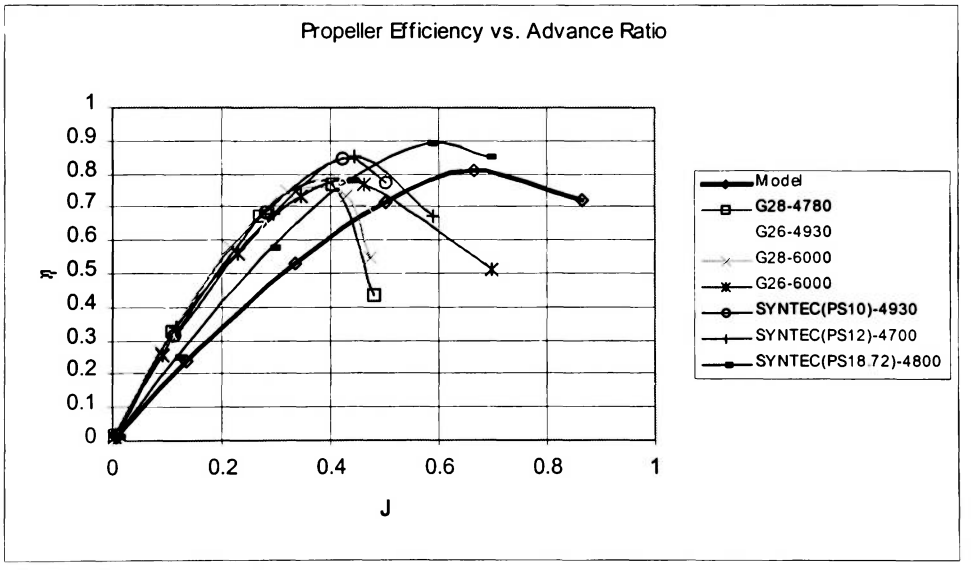

Figure 4E Propeller efficiency chart predicted by Rotor II

Appendix F: Detail drawings of the static engine test stand, and pictures

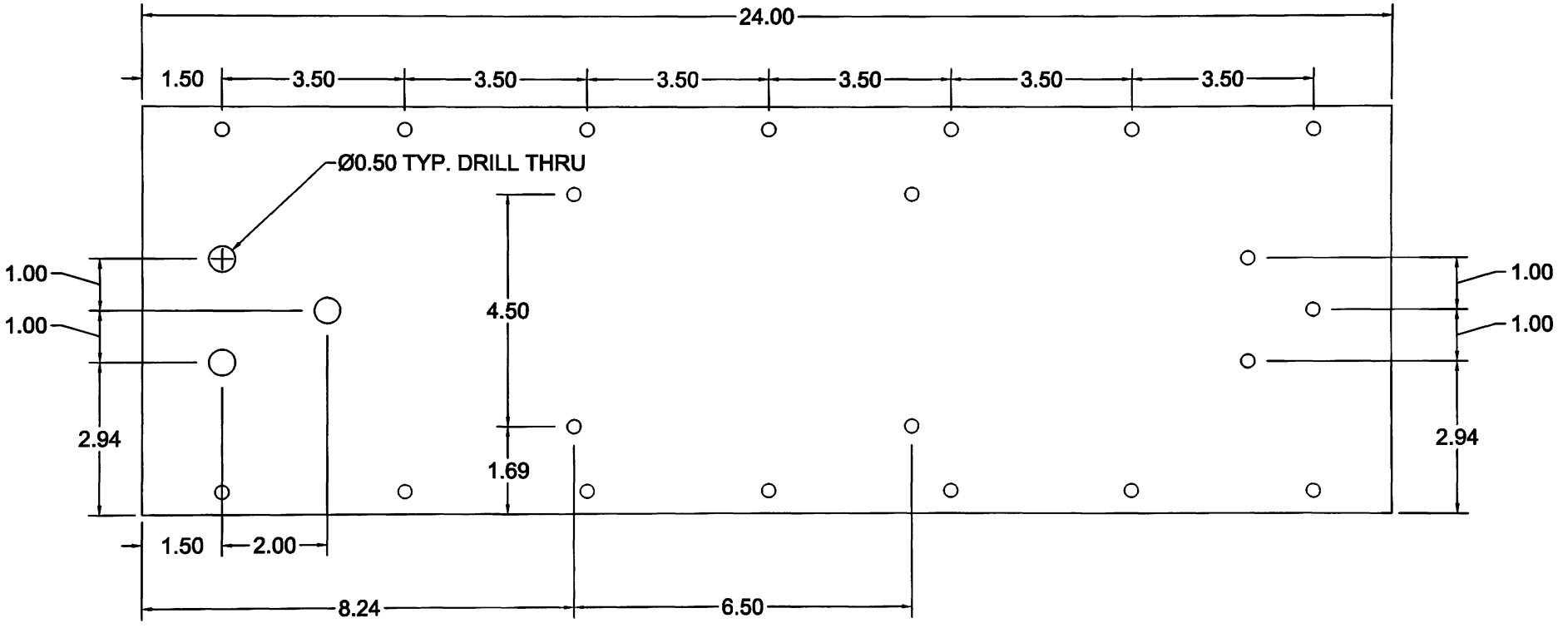

NOTE:
1. 0.25" THK ALUMINUM PLATE.
2. ALL HOLES Ø0.27" DRILL THRU UNLESS OTHERWISE SPECIFIED.

EMBRY-RIDDLE AERONAUTICAL UNIVERSITY
DAYTONA BEACH, FLORIDA 32114

TEST STAND PLATFORM

TOLERANCE
FRACTIONS: ±1/32
DECIMAL: ±0.01
ANGLES: ±1°
FINISH 125 RMS UNLESS OTHERWISE SPECIFIED.
BREAK EDGES 0.005MAX.
DO NOT SCALE DRAWING, ALL DIMENSIONS ARE IN INCHES.

SCALE: NOT TO SCALE
DRAWN BY: KENNETH HO, JF
CHECKED BY:
REVISED:
DATE: MARCH 28, 2008
DRAWING NO: 001

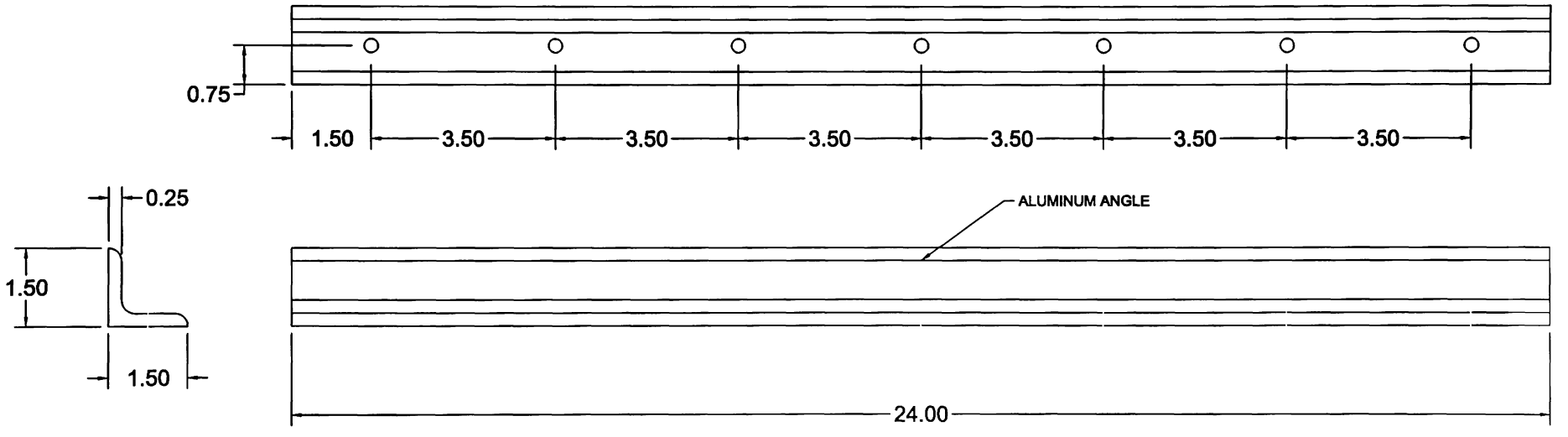

EMBRY-RIDDLE AERONAUTICAL UNIVERSITY
DAYTONA BEACH, FLORIDA 32114

TEST STAND PLATEFORM STIFFENER

TOLERANCE
FRACTIONS: ±1/32
DECIMAL: ±0.01
ANGLES: ±1°
FINISH 125 RMS UNLESS OTHERWISE SPECIFIED.
BREAK EDGES 0.005MAX.
DO NOT SCALE DRAWING, ALL DIMENSIONS ARE IN INCHES.

SCALE: NOT TO SCALE
DRAWN BY: KENNETH HO, JF
CHECKED BY:
REVISED:
DATE: MARCH 30, 2000
DRAWING NO: 002

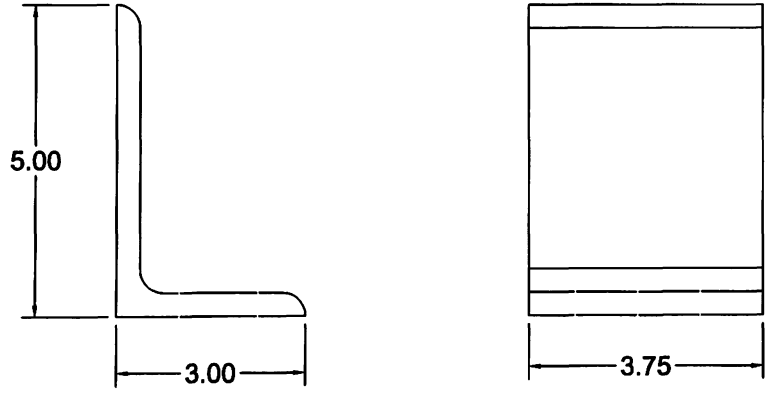

L-BRACKET

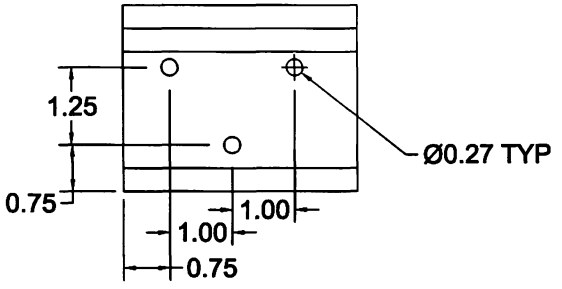

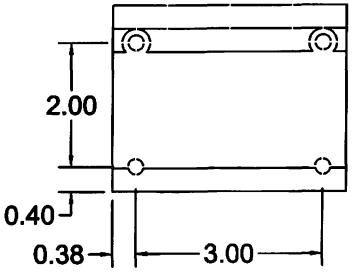

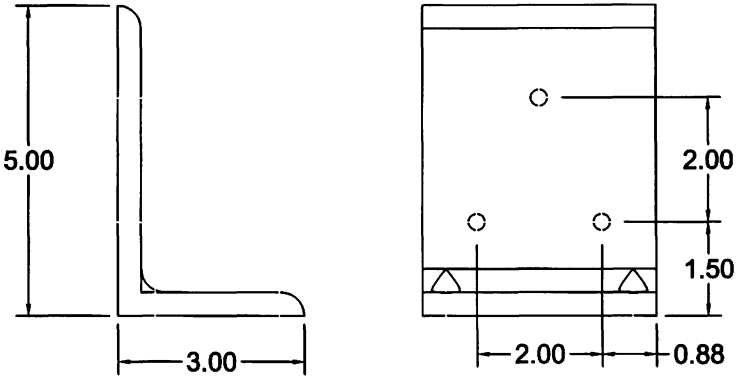

ENGINE MOUNT

EMBRY-RIDDLE AERONAUTICAL UNIVERSITY
DAYTONA BEACH, FLORIDA 32114

ENGINE MOUNT AND L-BRACKET

TOLERANCE
FRACTIONS: ±1/32
DECIMAL: ±0.01
ANGLES: 2°
FINISH 125 RMS UNLESS OTHERWISE SPECIFIED.
BREAK EDGES 0.005MAX.
DO NOT SCALE DRAWING, ALL DIMENSIONS ARE IN INCHES.

SCALE: NOT TO SCALE
DRAWN BY: KENNETH NO, JF
CHECKED BY:
REVISED:
DATE: MARCH 28, 2000
DRAWING NO: 003

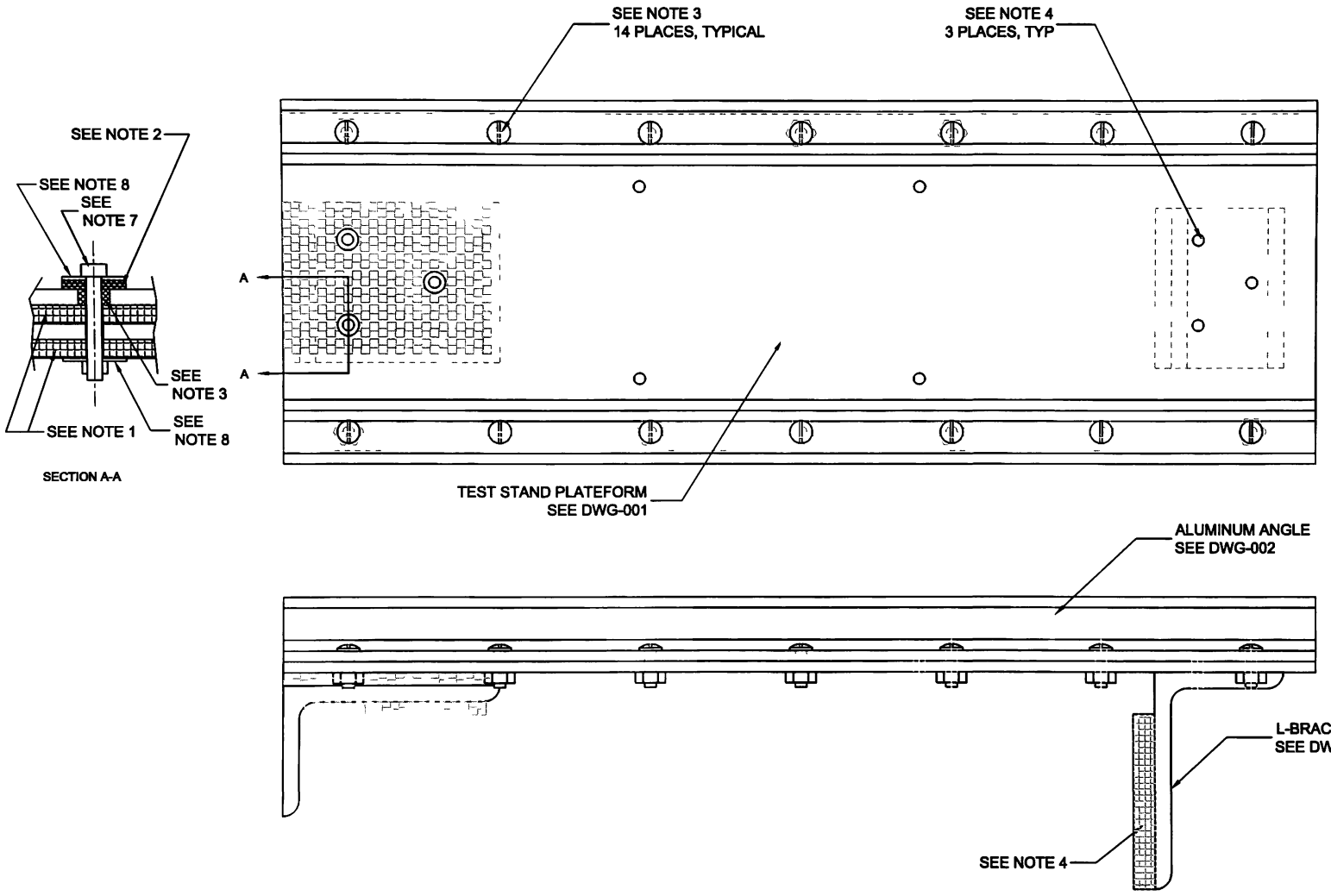

NOTE:
1. VIBRATION DAMPING MATERIAL
2. SOFT RUBBER MAT (1/16" THK)
3. 1/2" RUBBER O-RING
4. INSULATION MAT
5. 1/2" #10 BOLT WITH PHILIPS HEAD WITH NUT
6. 1" #10 BOLT WITH LOCK NUT
7. 1 1/2" #10 BOLT WITH LOCK NUT
8. 1" WASHER

EMBRY-RIDDLE AERONAUTICAL UNIVERSITY
DAYTONA BEACH, FLORIDA 32114

TEST STAND PLATFORM ASSEMBLY DRAWING

TOLERANCE
FRACTIONS: ±1/32
DECIMAL: ±0.01
ANGLES: ±1°
FINISH 125 RMS UNLESS OTHERWISE SPECIFIED.
BREAK EDGES 0.005MAX.
DO NOT SCALE DRAWING, ALL DIMENSIONS ARE IN INCHES.

SCALE: NOT TO SCALE
DRAWN BY: KENNETH HO, JF
CHECKED BY:
REVISED:
DATE: MARCH 30, 2000
DRAWING NO: 004

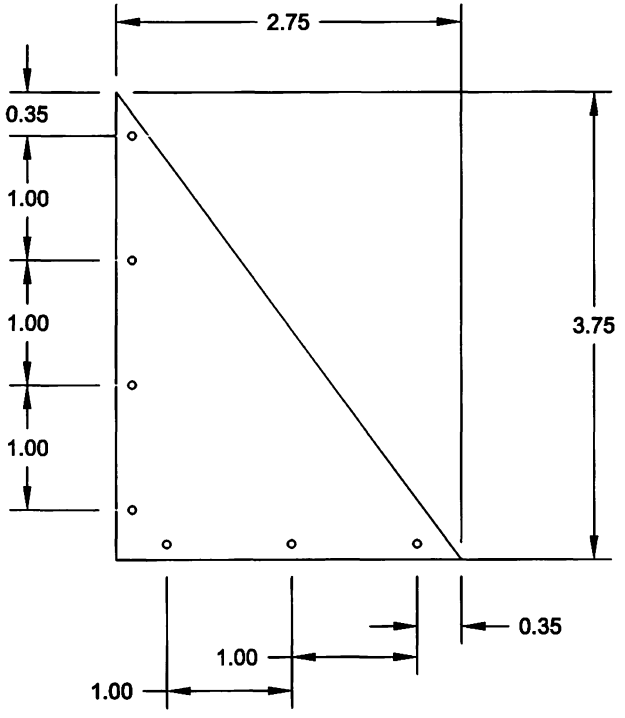

NOTE:
1/8" THK ALUMINUM PLATE
4 GAUSET PLATE, USED TO REINFORCE THE STRUCTURAL STIFFNESS OF THE EXISTING SAE STATIC THRUST ENGINE TEST STAND.

EMBRY-RIDDLE AERONAUTICAL UNIVERSITY
DAYTONA BEACH, FLORIDA 32114

GUASET PLATE

TOLERANCE
FRACTIONS: ±1/32
DECIMAL: ±0.01
ANGLES: ±1°
THREAD 125 RMS UNLESS OTHERWISE SPECIFIED.
BREAK EDGES 0.005MAX.
DO NOT SCALE DRAWING, ALL DIMENSIONS ARE IN INCHES.

SCALE: NOT TO SCALE
DRAWN BY: KENNETH NG, JF
CHECKED BY:
REVISED:
DATE: MARCH 28, 2000
DRAWING NO: 003

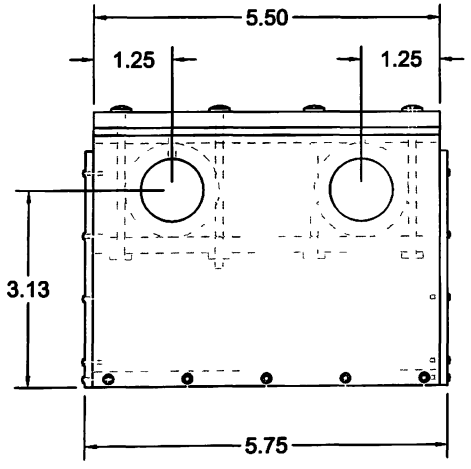

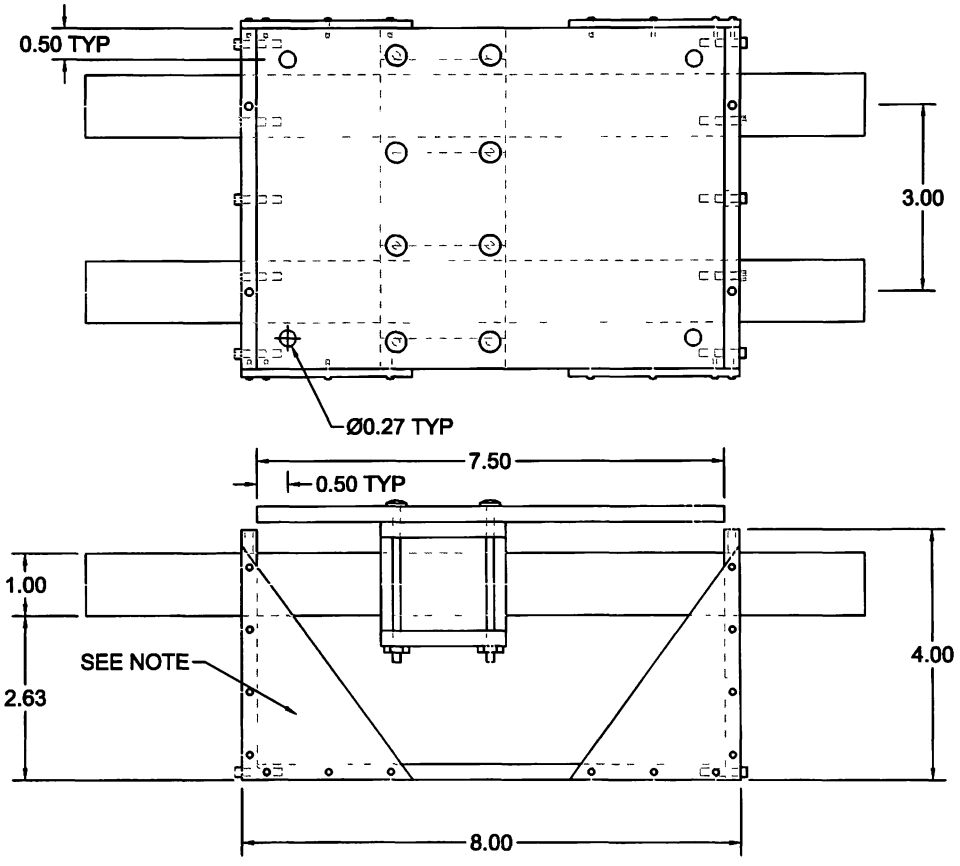

NOTE:
ALUMINUM GAUSET PLATE ADDED AT FOUR PLACES TO STRENGTHEN THE EXITISTING SAE STATIC THRUST ENGINE TEST STAND.
DETAILS SEE DWG-005

EMBRY-RIDDLE AERONAUTICAL UNIVERSITY
DAYTONA BEACH, FLORIDA 32114

SAE STATIC THRUST ENGINE TEST STAND

TOLERANCE
FRACTIONS: ±1/32
DECIMALS: ±0.01
ANGLES: ±1°
FINISH 125 RMS UNLESS OTHERWISE SPECIFIED.
BREAK EDGES 0.010MAX.
DO NOT SCALE DRAWING, ALL DIMENSIONS ARE IN INCHES.

SCALE: NOT TO SCALE
DRAWN BY: KENNETH NG, JF
CHECKED BY:
REVISED:
DATE: MARCH 30, 2000
DRAWING NO: 000

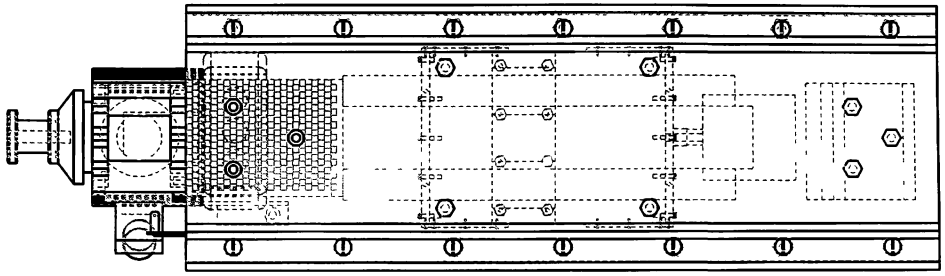

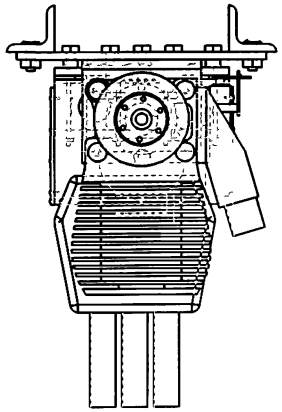

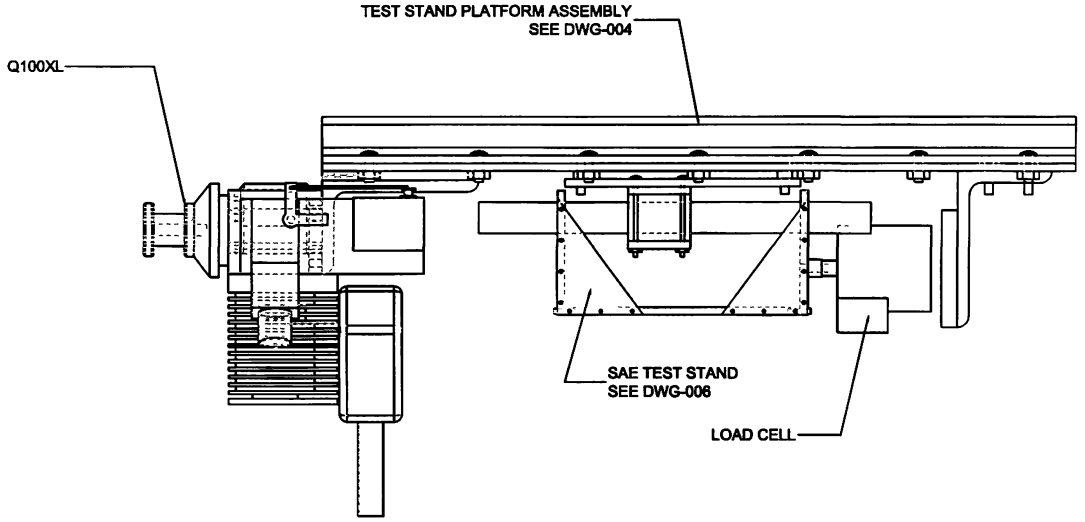

EMBRY-RIDDLE AERONAUTICAL UNIVERSITY
DAYTONA BEACH, FLORIDA 32114

STATIC THRUST ENGINE TEST STAND ASSEMBLY DRAWING

TOLERANCE
FRACTIONS: ±1/32
DECIMALS: ±0.01
ANGLES: ±1°
FINISH 125 RMS UNLESS OTHERWISE SPECIFIED.
BREAK EDGES 0.005MAX.
DO NOT SCALE DRAWING, ALL DIMENSIONS ARE IN INCHES.

SCALE: NOT TO SCALE
DRAWN BY: KENNETH HO, JF
CHECKED BY:
REVISED:
DATE: MARCH 30, 2000
DRAWING NO: 007

Figure 1F Static thrust engine test stand developed for this research

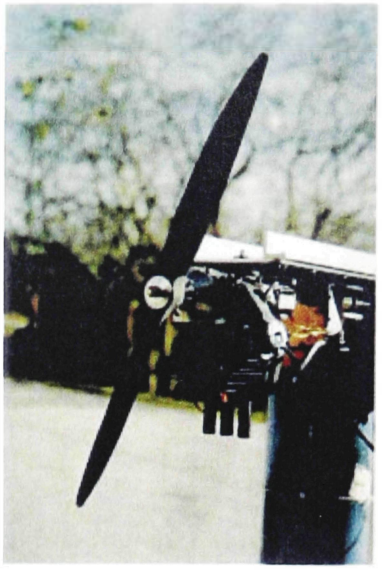

Figure 2F Closeup view of the engine installed on the test stand

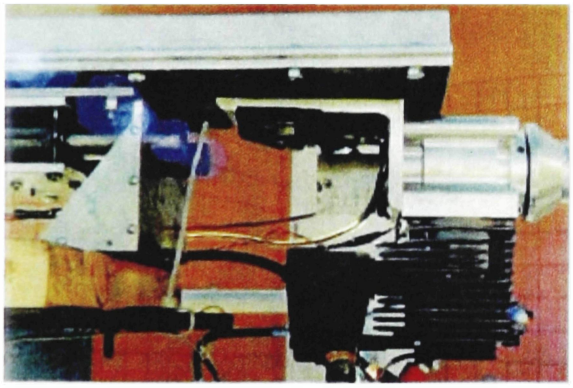

Figure 3F Installing damping material between the engine mount and the stand to minimize the vibration of the engine

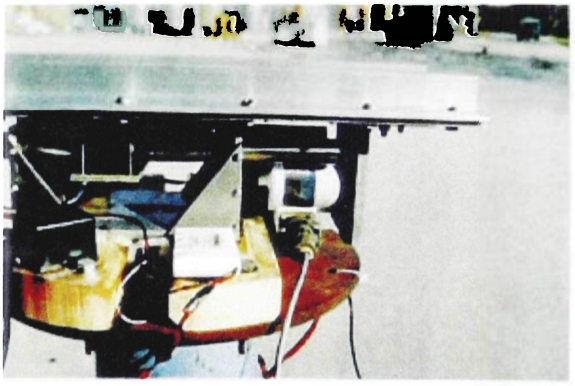

Figure 4F A foam pad was installed in between the Load cell and the L-bracket

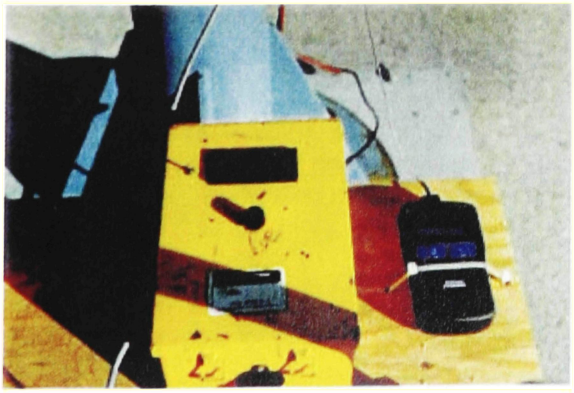

Figure 5F Load scale (left) and Temperature scale (right)

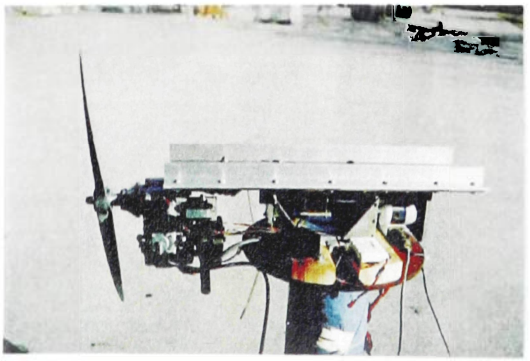

Figure 6F Full side view of the static thrust engine test stand

Appendix G: Pictures of the model at different construction stages

Figure 1G Data acquisition system range and interference check at ERAU soccer field

Figure 2G Data acquisition system range check, and interference check at different view angle

Figure 3G Attached fiberglass skin to the model (side view)

Figure 4G Working on the fairing between windshield and wing fairing

Figure 5G Working on fuselage transition between the wing root and the rear windshield

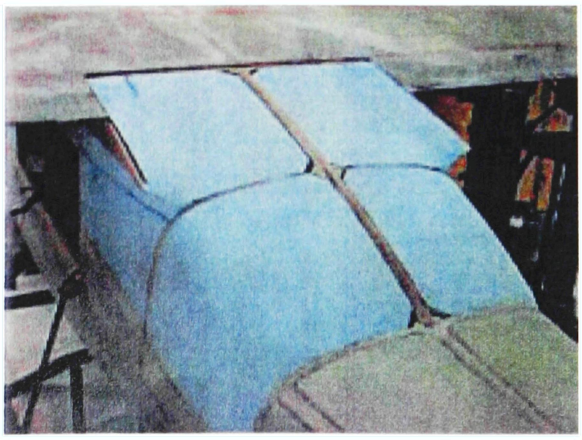

Figure 6G Working on fuselage transition between the wing root and the rear windshield (different view angle)

Figure 7G Wing struts and Flaps

Figure 8G The model was ready for the first coat of primer

Figure 9G Model with 3 coat of primer

Figure 10G Model at different view angle